A salt bridge mediated resistance mechanism to FtsZ inhibitor PC190723 revealed by a single step cell-based screen

Ajay Kumar Sharma[1,2,3], Sakshi Mahesh Poddar[1,2,3], Joyeeta Chakraborty[4], Bhagyashri Soumya Nayak[1,2,3], Srilakshmi Kalathil[1,2,3], Nivedita Mitra[1,2,3], Gayathri Pananghat[4‡] and Ramanujam Srinivasan[1,2,3‡]

[1] School of Biological Sciences, National Institute of Science Education and Research, Bhubaneswar – 752050, India

[2] Homi Bhabha National Institutes (HBNI), Training School Complex, Anushakti Nagar, Mumbai, India 400094

[3] Centre for Interdisciplinary Sciences, National Institute of Science Education and Research, Bhubaneswar, India 752050

[4] Biology, Indian Institute of Science Education and Research, Pune – 411008, India

[‡] Corresponding authors

e-mail: rsrini@niser.ac.in; gayathri@iiserpune.ac.in

Abstract:

Bacterial cell division proteins, especially the tubulin homolog FtsZ, have emerged as strong targets for developing new antibiotics. Several assays have been designed to screen for small molecules targeting FtsZ but rely upon a multitude of steps to validate the target and to ensure minimum toxicity to the eukaryotic cells. Here, we have utilized the fission yeast heterologous expression system to develop a single step cell-based assay to screen for small molecules that directly and specifically target the bacterial cell division protein FtsZ and are non-toxic to eukaryotic cells. As a proof-of-concept of the utility of this assay, we demonstrate the effect of the inhibitors sanguinarine, berberine and PC190723 on FtsZ. Though sanguinarine and berberine affect FtsZ polymerization, they exert a toxic effect on the cells. Further, using this assay system, we show that PC190723 affects *Helicobacter pylori* FtsZ function and gain new insights into the molecular determinants of resistance to PC190723. Based on sequence and structural analysis and site-specific mutations, we demonstrate that the presence of salt-bridge interactions between the central H7 helix and beta-sheet S10 and S7 mediate resistance to PC190723 in FtsZ. The single step *in vivo* cell-based assay using fission yeast enabled us to dissect the contribution of sequence-specific features of FtsZ and cell permeability effects associated with bacterial cell envelopes. Thus, our assay functions as a powerful tool to rapidly identify new molecules that specifically target the bacterial cell division protein FtsZ, or other polymeric bacterial cytoskeletal proteins, understand how they affect polymerization dynamics and study resistance determinants in targets.

Running Title: A salt bridge in FtsZ mediates resistance to PC190723

Keywords: FtsZ, PC190723, antimicrobial resistance, bacterial cytoskeleton, fission yeast

Introduction:

The rapid emergence and spread of antibiotic resistance, to almost every antibiotic currently in use against bacteria, has resulted in an urgent need to develop new classes of antibiotics. While the existing antibiotics target DNA replication, protein synthesis and cell wall synthesis, several antibiotics in the pipeline have new targets with a novel mechanism of action to overcome the emerging resistance problem (Butler and Paterson, 2020). One of the most potential target candidates is FtsZ, an essential bacterial cell division machinery protein (Carro, 2019; Schaffner-
Barbero et al., 2012; Silber et al., 2020; Wang et al., 2003).

FtsZ is a prokaryotic homolog of tubulin, which is highly conserved and present in all bacteria and many archaea
(Addinall and Holland, 2002; Erickson, 1995; Erickson et al., 2010; Margolin, 2005; Nogales et al., 1998; Vaughan et al., 2004). FtsZ monomers self-assemble into polymeric structures in presence of GTP to give rise to FtsZ protofilaments *in vitro* and assemble into the so-called Z-ring at the division site *in vivo*. The Z- ring is the first structure to be assembled at the division site and is responsible for the recruitment of more than a dozen other accessory proteins which comprise the divisome, the division apparatus of the cell (Bi and Lutkenhaus, 1991; Bramhill and Thompson, 1994; Huang et al., 2013; Ma et al., 1996; RayChaudhuri and Park, 1992; Weiss, 2004; Weiss et al., 1999). The Z-ring is a highly dynamic structure with a half-life of less than 10 seconds due to the constant exchange of FtsZ molecules between the ring and the soluble monomers
(Anderson et al., 2004). Since the Z-ring lies at the core of the cell division process, its functional defects result in bacterial growth inhibition and cell death
(Addinall and Lutkenhaus, 1996; Barrows and Goley, 2021; Mahone and Goley, 2020; Vollmer, 2006; Zorrilla et al., 2021). For example, abrogating FtsZ function using FtsZ

polymer stabilizer PC190723 is protective against *Staphylococcus aureus* infections in mouse models (Haydon et al., 2008).

FtsZ has three important protein pockets that bind the small molecules and are collectively known as druggable regions. These regions are the nucleotide-binding domain (NBD), the inter-domain cleft (IDC) present between the central core helix (H7 helix) and the C- terminal domain (CTD) and the T7 loop (Kusuma et al., 2019; Löwe and Amos, 1998). The T7 loop of one subunit is inserted into the NBD of another subunit of FtsZ to form a catalytic site for GTP hydrolysis **(Fig. 1A)**. Several small molecules have been shown to target FtsZ, which include heterocyclic molecules like guanidinomethyl biaryl compounds (Kaul et al., 2012), N-heterocycles such as Zantrin Z5 (Margalit et al., 2004), 3-phenyl substituted 6,7-dimethoxyisoquinoline (Kelley et al., 2012), benzamides (Adams et al., 2011; Haydon et al., 2008; Straniero et al., 2017, 2020) and trisubstituted benzimidazoles (Kumar et al., 2011). These and several other derivatives with the potential to be used as antibacterial drugs are berberine **(Fig. 1, *inset* i)** and sanguinarine **(Fig. 1, *inset* ii)**. Berberine binds to FtsZ at a 1:1 ratio *in vitro* and exhibits dose-dependent inhibition of FtsZ assembly kinetics with a reduction in GTPase activity. Berberine is believed to target the GTP-binding pocket in the FtsZ structure and further affects the FtsZ polymer stability and Z- ring formation *in vivo* (Boberek et al., 2010; Domadia et al., 2008; Pradhan et al., 2021; Sun et al., 2014). Sang uinarine, also thought to bind the nucleotide-binding domain (NBD) in FtsZ, prevents bundling of FtsZ protofilaments *in vitro* and perturbs the Z- ring assembly *in vivo* (Beuria et al., 2005). The precise mechanism of inhibition or the binding site of these drugs remains unclear.

The most potent and promising among the FtsZ inhibitors is PC190723 **(Fig. 1, *inset* iii)**, a 2,6-difluorinated 3-methoxybenzamide derivative

(Haydon et al., 2008). PC190723, which binds at the inter-domain cleft of FtsZ, remains the only drug whose target site in FtsZ is clearly established **(Fig. 1)**. Crystal structures of FtsZ from *S. aureus* with PC190723 show that the drug occupies the inter-domain cleft between the central core helix (H7 helix) and the C-terminal domain (Matsui et al., 2012). PC190723 binds preferentially to the T state of *S. aureus* FtsZ in which the cleft remains open, thus stabilizing the high-affinity conformation required for FtsZ polymer elongation (Fujita et al., 2017; Matsui et al., 2012). Thereby, PC190723 reduces the critical concentration for polymerization and induces FtsZ assembly (Andreu et al., 2010; Elsen et al., 2012). Although the resistance of streptococci, enterococci and many Gram –ve bacteria to PC190723 (Haydon et al., 2008; Kaul et al., 2013a) and poor drug and pharmacokinetic properties have hampered the pre-clinical trials with PC190723 (Kaul et al., 2013b; Stokes et al., 2013), phase-I tests are in progress by TAXIS pharmaceuticals (Monmouth Junction, NJ, USA) for the benzamide class of drug TXA709 (Butler and Paterson, 2020; TAXIS Pharmaceuticals, 2020).

Thus, despite several years of intense research on FtsZ inhibitors, a commercially viable antibiotic that targets FtsZ is not yet available. One of the major hindrances has been the validation that FtsZ is the actual direct target of these small molecule compounds (Kusuma et al., 2019). Although several other small molecules have been shown to inhibit bacterial cell division, presumably due to directly inhibiting FtsZ function, many of them have also been shown to be due to indirect effects on membranes (Hurley et al., 2016). Several methods have been used to ascertain FtsZ as the target of the drug. While *in vitro* biochemical assays are useful to find molecules that directly target FtsZ, they are cumbersome and need to be performed at optimal physiological pH and ionic conditions, which can be considerably variable among FtsZ from different species. A scheme of methods to be followed, from the identification of hit compounds to the

development of a lead compound, has also been proposed (Schaffner-Barbero et al., 2012). The advantages and disadvantages of each of these methods have been reviewed in detail by Kusuma et al (2019). These include several assays starting with testing FtsZ polymerization to the sensitivity of eukaryotic cells. Any small molecule antagonist identified thus should have no off-target effects and minimally affect eukaryotic cells. A single step screening method that identifies small molecules, directly targeting FtsZ assembly and as well as selects out compounds probably toxic to eukaryotic cells would be ideal. Moreover, the screen should be easily scalable to high-throughput platforms.

We had previously established *Schizosaccharomyces pombe* as a useful model system to study bacterial cytoskeletal proteins. We had shown that A22, a small molecule inhibitor of the actin homologue, MreB, prevented its polymerization in yeast cells as well (Srinivasan et al., 2007). Further, we reported that FtsZ assembles into ring-like structures with similar characteristics to Z-rings in bacterial cells when expressed in *S. pombe* or *Saccharomyces cerevisiae* (Srinivasan et al., 2008). These observations prompted us to explore if the heterologous expression system using *S. pombe* could serve as a platform for testing and screening chemical compounds targeting FtsZ directly. In this study, we show that FtsZ from two pathogenic bacterial species, *S. aureus* and *Helicobacter pylori*, expressed in fission yeast, assemble into dynamic ring-like and spiral polymers, respectively. We test the effect of known small molecule inhibitors of FtsZ, sanguinarine, berberine and PC190723 on the assembly of FtsZ polymers. Herein, we thus develop a proof-of-concept of a cell-based screening method that is easily scalable to existing high-throughput platforms. The method combines the ability to establish the specificity of the target by directly assaying the polymerization of FtsZ in the cellular milieu as well as assessing the eukaryotic toxicity in a single step **(Fig. 2)**. We find that although sanguinarine and berberine affected FtsZ polymerization, they also affected eukaryotic cell

physiology. We show that while all three drugs exert an effect on FtsZ assembly, PC190723 specifically promotes the assembly of FtsZ polymers of *S. aureus* and *H. pylori*. Further, we probed the determinants of resistance to PC190723 based on FtsZ sequence and structure analysis and show that a salt-bridge interaction between the central H7 helix and S10 β-sheet prevents the drug from accessing the inter-domain cleft (IDC). This appears to be a mechanism of resistance probably prevalent in many Gram –ve bacteria. We thus demonstrate the utility of the heterologous yeast system (*S. pombe*) for identifying chemical compounds directly targeting FtsZ while being non-toxic to eukaryotic cells and studying the molecular determinants of drug resistance.

Results:

S. aureus and H. pylori FtsZ assemble into polymeric structures in fission yeast

We expressed FtsZ from two pathogenic species, *S. aureus* and *H. pylori*, hereafter referred to as SaFtsZ for *S. aureus* FtsZ and HpFtsZ for *H. pylori* FtsZ, respectively as C-terminal GFP fusions in *S. pombe*. Expression of FtsZ in *S. pombe* was achieved from a pREP42-GFP vector (a medium strength thiamine repressible promoter *nmt41/42* containing vector; (Basi et al., 1993; Moreno et al., 2000) by growing cultures in minimal medium in the absence of thiamine (induction medium) as reported earlier (Srinivasan et al., 2008). Epifluorescence microscopy showed that SaFtsZ assembled predominantly into spot-like structures (**Fig. 3A**) and were similar in appearance to that assembled by FtsZ from *Escherichia coli* (EcFtsZ) **(Fig. 3B)**. Assembly of SaFtsZ into ring-like structures was only discernible by super-resolution microscopy using structural illumination (3D-SIM) **(Fig. 3C)**, whereas ring-like structures of EcFtsZ were visualized by deconvolution of images **(Fig. 3B iii)**. Interestingly, HpFtsZ assembled into cable-like structures (**Fig. 3D**) that were curled and spiral in appearance that was more clearly visualized by deconvolution of the images (**Fig. 3D iii and 3E**). Further, super-resolution

imaging using 3D-SIM clearly revealed that HpFtsZ assembled into spiral filaments (**Fig. 3F**). These results show that FtsZ from both species *S. aureus* (SaFtsZ) and *H. pylori* (HpFtsZ), when expressed in fission yeast cells, like many other FtsZ, assemble into polymeric structures.

Sanguinarine and berberine prevent FtsZ assembly in fission yeast, but also affect yeast cell morphology

Sanguinarine and berberine have been shown to perturb FtsZ ring assembly in *E. coli* (Beuria et al., 2005; Boberek et al., 2010; Domadia et al., 2008; Liu et al., 2017). Although sanguinarine has been reported to inhibit septation and cell division in *S. aureus* (Obiang-Obounou et al., 2011), its effects on SaFtsZ or HpFtsZ have not yet been reported. We, therefore, tested if any of these molecules that have been shown to prevent FtsZ ring assembly in bacteria exhibited any direct effects on FtsZ expressed in yeast cells.

A microscopic examination of fission yeast cells expressing SaFtsZ **(Fig. 4A)**, EcFtsZ **(Fig. 4B)** or HpFtsZ **(Fig. 4C)** in the presence of sanguinarine **(Fig. 4 A ii – C ii)** or berberine **(Fig. 4 A iii – C iii)** revealed that assembly of FtsZ into polymers was inhibited in the presence of the drugs as compared to untreated (DMSO added) cells **(Fig. 4 A i – C i)**. Quantification of the number of cells (≥ 500 cells counted for each replicate; N = 3) showed a reduction in the percentage of cells that exhibited FtsZ assemblies (spots/ dots in the case of SaFtsZ or EcFtsZ and filaments in the case of HpFtsZ) in the presence of sanguinarine or berberine as compared to control untreated cells **(Fig. 4 D i – iii and E i – iii)**. In the case of sanguinarine, the difference of means (effect size) in the proportion of cells containing FtsZ polymers between treated and untreated (DMSO) cells were 16.9 [95% CI 9.5, 24.2], 23 [95% CI 20.6, 25.4] and 17.5 [95%CI 13.7, 21.4] for SaFtsZ, HpFtsZ and EcFtsZ respectively. The difference of means (effect size) in the proportion of cells

containing FtsZ polymers between cells treated with berberine and untreated (DMSO) cells were 22.4 [95% CI 15.8, 29.0], 22.1 [95% CI 18.6, 25.6] and 18.9 [95% CI, 16.1, 21.6] for SaFtsZ, HpFtsZ and EcFtsZ respectively. These results suggest that sanguinarine and berberine had an effect on the assembly of FtsZ from all three species, *S. aureus*, *H. pylori* and *E. coli* when expressed in fission yeast cells. However, at higher concentrations, both sanguinarine (135.95 μM) and berberine (134.45 μM) induced significant morphological defects in yeast cells **(Fig. 4F)**.

Further, in order to test if the effects of sanguinarine and berberine were specific to FtsZ polymerization, we tested its activity on the *E. coli* actin homologue MreB. Sanguinarine and berberine showed no effects on MreB assembly **(Fig. S1 iii and iv)**. However, A22, a known inhibitor of MreB (Gitai et al., 2005; Iwai et al., 2002), as previously reported (Srinivasan et al., 2007), completely inhibited the polymerization of EcMreB in fission yeast **(Fig. S1 ii)**.

PC190723 induces polymerization of both SaFtsZ and HpFtsZ, but not EcFtsZ

Several studies have shown that PC190723 binds SaFtsZ, and crystal structures have revealed the binding site to be the inter-domain cleft on FtsZ (Haydon et al., 2008; Matsui et al., 2012; Tan et al., 2012). Further, PC190723 preferentially binds to the T state of SaFtsZ, inhibits the GTPase activity of FtsZ, induces polymerization and stabilizes FtsZ filaments (Andreu et al., 2010; Elsen et al., 2012; Fujita et al., 2017; Miguel et al., 2015). We, therefore, decided to test PC190723 for its effects on SaFtsZ, HpFtsZ and EcFtsZ expressed in fission yeast cells. We first tested the effect of PC190723 at various concentrations (ranging from 5 μg/ mL to 25 μg/ mL) on the assembly of FtsZ polymers. At 8 – 10 hours after growth in the induction medium (EMM without thiamine), the majority of cells expressing SaFtsZ or HpFtsZ showed only diffuse FtsZ molecules in

the cytoplasm and had not yet assembled into structures. PC190723 or DMSO was added to cultures at this point and incubated at 30°C for further 4 hours. In cultures where DMSO was added, 446 ± 5 (SEM; 500 cells counted for each replicate; N = 3) cells expressing SaFtsZ **(Fig. 5 A and B ii)** and 378 ± 4 (SEM; 500 cells counted for each replicate; N = 3) cells expressing HpFtsZ **(Fig. 5 C and D ii)** were found to have only diffuse FtsZ molecules in the cytoplasm.

On the contrary, cultures treated with PC190723 (12.5 μg / mL or more) had a significantly more proportion of cells with FtsZ assembled into polymers as compared to untreated cells (DMSO) for SaFtsZ **(Fig. 5 A and B iv)** and HpFtsZ **(Fig. 5 C and D iv)**. Nearly 80.5 ± 2.5 % (95% CI; N = 3) of cells (403 ± 3, SEM; 500 cells counted for each replicate; N = 3) had patches/ spots of SaFtsZ when treated with 20 μg / mL (56.2 μM) PC190723 as compared to a mere 10.8 ± 4.3 % (95% CI; N = 3) in untreated (DMSO) cells (54 ± 5, SEM; cells 500 counted for each replicate; N = 3) **(Fig. 5A)**. At 20 μg/ mL of PC190723, the effect size was 69.7 [95%CI 66.2, 73.2]. In the case of HpFtsZ, nearly 24.3 ± 3.01 % (95% CI; N = 3) of untreated cells (122 ± 4, SEM; 500 counted for each replicate; N = 3) had FtsZ filaments, and in the presence of 20 μg / mL (56.2 μM) of PC190723, the number of cells having HpFtsZ filaments increased to 68.07 ± 6.55 % (95% CI; N = 3, i.e. 340 ± 8, SEM; 500 counted for each replicate) **(Fig. 5C)**. The effect size was 43.7 [95%CI, 38.7, 48.7]. Further, with an increasing concentration of PC190723, there was a concomitant increase in the proportion of cells that contained polymerized FtsZ in the case of SaFtsZ **(Fig. 5A)** and HpFtsZ **(Fig. 5C)**. However, no such difference was observed in the absence or presence of PC190723 in cells expressing EcFtsZ **(Fig. 5E and F)** and is consistent with a recent study that concluded that the inhibitory activity of PC190723 on *E. coli* was independent of FtsZ (Khare et al., 2019). These observations suggested that PC190723 resulted in an early assembly of FtsZ into polymers in the case of SaFtsZ and HpFtsZ, but it did not act on EcFtsZ. Further, the addition of PC190723

after the appearance of FtsZ polymers in yeast cells did not have any notable effect on the FtsZ structures **(Fig. S2 A – C)**. Our results presented here thus support the earlier reports that PC190723 acts to reduce the critical concentration of FtsZ polymerization of SaFtsZ (Andreu et al., 2010; Elsen et al., 2012).

PC190723 stabilizes polymers and slows down the turnover rates of both SaFtsZ and HpFtsZ

We tested if PC190723 impacted the turnover rates of SaFtsZ and HpFtsZ using fluorescence recovery after photobleaching (FRAP) experiments. Fluorescence recovery was measured after bleaching a complete SaFtsZ spot or patch either in untreated cells **(Fig. 6A)** or in cells treated with 20 μg / mL (56.2 μM) of PC190723 **(Fig. 6B)**. Representative graphs showing the fluorescence recovery of SaFtsZ in the absence of PC190723 or the presence of 20 μg / mL (56.2 μM) of PC190723 are depicted in **Figure 6C** and **Figure 6D,** respectively, and the plots for all such cells are shown **(Fig. S3 A and B)**. While SaFtsZ exhibited rapid dynamics with a half-time ($t_{1/2}$) of 3.61 ± 0.41 seconds (95% CI; N = 10) in the absence of PC190723, the half-time ($t_{1/2}$) of fluorescence recovery increased by nearly 3-fold to 11.34 ± 3.52 seconds (95% CI; N = 10) in the presence of PC190723 **(Fig. 6E)**, giving an effect size of 7.7 [95% CI 4.0, 11.5]. Fluorescence recovery of HpFtsZ was similarly measured after bleaching a small part of HpFtsZ filaments either in untreated cells **(Fig. 6F)** or in cells treated with 20 μg / mL (56.2 μM) of PC190723 **(Fig. 6G)**. Representative graphs of the fluorescence recovery of HpFtsZ in the absence of PC190723 or the presence of 20 μg / mL (56.2 μM) of PC190723 are shown in **Figure 6H** and **Figure 6I,** respectively. The plots for all such cells are shown **(Fig. S3 C and D).** The effect of PC190723 on the turnover rates of HpFtsZ was milder but significant and resulted in 1.96 times fold change in the fluorescence recovery half-time ($t_{1/2}$) rates with an effect size of 5.9 [95% CI 3.5, 8.3]. The recovery half-time ($t_{1/2}$)

was 6.16 ± 0.89 seconds (95% CI; N = 10) in untreated cells and is consistent with the earlier reports (Specht et al., 2013). In the presence of PC190723, it increased to 12.06 ± 2.14 seconds (95% CI; N = 10) **(Fig. 6J)**. These results from the FRAP studies show that PC190723 affects the dynamics and turnover of both *S. aureus* and *H. pylori* FtsZ filaments, consistent with an effect of stabilization of filaments by the inhibitor.

SaFtsZ^{G196A} and HpFtsZ^{G213A} expressed in yeast exhibit PC190723 resistance

A comparison of the FtsZ sequences from various bacterial species that were tested for growth inhibition by PC190723 had revealed several key residues in FtsZ, determining its susceptibility/ resistance (Haydon et al., 2008). In both *B. subtilis* and *S. aureus*, a single point mutation in FtsZ at G196 position to alanine (A) has been shown to result in a several-fold increase in the minimal inhibitory concentration of PC190723 (Stokes et al., 2013). Therefore, we next tested if we could experimentally observe resistance to PC190723 by FtsZ mutants G196A in our yeast expression system. Structure-based sequence alignment and comparisons showed that the equivalent residue of G196 in HpFtsZ is G213 and is conserved across the FtsZs **(Fig. S4)**. Hence we changed G213 in HpFtsZ to alanine (Ala) and expressed HpFtsZ^{G213A} in fission yeast. We then tested the effect of PC190723 on the mutation in a similar manner as described above, at a point when untreated cells predominantly exhibited diffuse fluorescence or short polymers.

In the case of HpFtsZ^{G213A}, we found that only 41 ± 2.9 % (95% CI; N = 3; 500 cells were counted for each replicate) of the cells treated with 20 μg / mL (56.2 μM) PC190723 as compared to 31 ± 16.4 % (95% CI; N = 3; 500 cells were counted for each replicate) in untreated cells had FtsZ polymers **(Fig. 7 A – C)**. As compared to the effect size of 28.2 [95% CI 19.8, 36.7] for HpFtsZ^{WT}, the effect size for HpFtsZ^{G213A} treated with PC190723 was 10.4 [95% CI -1.1, 21.9] with a negative value for the lower bound. Thus, there was

no significant increase in the number of cells having FtsZ polymers in the mutant HpFtsZ^{G213A} upon treatment with PC190723 **(Fig. 7A)**. In comparison, as described above, HpFtsZ^{WT} exhibited a significant increase in the number of cells having FtsZ polymers (70% of cells) when treated with PC190723 (**Fig. 7A and 5C**). Although PC190723 did not have an effect on the G213A mutant of HpFtsZ, HpFtsZ^{G213A} was proficient in polymerization and assembled into filaments **(Fig. S5A)**. We also expressed SaFtsZ^{G196A} in fission yeast cells from the same *nmt41/42* promoter as for the wild-type SaFtsZ. Surprisingly, unlike HpFtsZ^{G213A}, we found that SaFtsZ^{G196A} failed to assemble into any structures in yeast cells **(Fig. S5B ii)**. Although it has been shown that FtsZ^{G196A} is functional for cell division in both *S. aureus* and *B. subtilis* and forms Z-rings in the latter (Adams et al., 2016; Haydon et al., 2008; Stokes et al., 2013), mutations at G196 is also known to result in growth defects in *S. aureus*
(Adams et al., 2016; Stokes et al., 2013). Nonetheless, the addition of 20 μg / mL (56.2 μM) of PC190723 also did not induce any polymerization of assembly of SaFtsZ^{G196A} **(Fig. S5B iv)**. Taken together, our results show that mutations that render FtsZ insensitive to PC190723 do not assemble early into polymeric structures in the presence of the drug, suggesting that PC190723 fails to bind SaFtsZ^{G196A} and HpFtsZ^{G213A}.

PC190723 docks into the inter-domain cleft of HpFtsZ **modelled structure** ***in the T state***

Crystal structures of SaFtsZ bound with PC190723 **(Fig. 8A and B; PDB ID 4DXD)** reveal the binding mode of PC190723 to the T state conformation of the protein **(Matsui et al. 2012; Tan et al. 2012).** In the T state conformation of FtsZ, the cleft between NBD and CTD is opened, and hence the drug can be accommodated in the pocket. The residues Gly196, Leu200, Val203, Asn208, Leu209, Met226, Ile228, Asn263, Val297, Thr309 and Ile311 interact with the drug in SaFtsZ **(Fig. 8A)**. In the R state conformation of FtsZ, the

cleft between NBD and CTD is closed and hence does not have an adequate gap between the H7 helix and the central beta-sheet of CTD (S8 and S9 strands) to accommodate PC190723 into the cleft. The drug shows clashes with residues of the cleft when the T state structure (PDB ID: 4DXD) is superimposed with the R state structure (PDB ID: 5H5I) of SaFtsZ **(Fig. 8B)**. A structure-based multiple sequence alignment reveals that many of the residues in FtsZ involved in the interaction with PC190723 are conserved in HpFtsZ **(Fig. S4 A and B)**.

We further resorted to *in silico* approaches to determine if the inter-domain cleft in HpFtsZ could accommodate PC190723. We thus modelled HpFtsZ using the SwissModeller (Waterhouse et al., 2018) with the T state of SaFtsZ as a template and superposed it with the PC190723 bound SaFtsZ structure (4DXD) to see whether PC190723 can fit into the modelled HpFtsZ structure **(Fig. 8C)**. Analysis of PC190723 in the inter-domain cleft of the HpFtsZ model indicated that several residues that made direct contact with the drug in the crystal structure of the PC190723-SaFtsZ complex (4DXD) were conserved in HpFtsZ and shown to be within interacting distances of PC190723. Phe281 of HpFtsZ could potentially interact by stacking interaction with the ring of PC190723. The side chain of Thr328 is at a distance capable of forming hydrogen bonds, while the side chain of Ile217 forms van der Waals interaction with the inhibitor **(Fig. 8C and Fig. S4, B)**. Unlike in the R state, the residues in the S7, S9 and S10 beta-sheets or the H7 helix do not clash with the inhibitor in the T state.

Resistance to PC190723 is mediated by salt-bridge interactions that prevent drug binding in the inter-domain cleft.

A single point mutation in FtsZ at position Gly196 in *B. subtilis* and *S. aureus* is sufficient to render them resistant to PC190723. However, it was also noted that while the

susceptible species were characterized by the presence of valine (Val) at position 307, some other species of bacteria that were naturally resistant to PC190723 contained arginine (Arg) or histidine (His) at this position
(Haydon et al., 2008; Kaul et al., 2013a). Surprisingly, HpFtsZ contains an arginine at this position (Arg326), and yet our results from the yeast expression studies suggested that PC190723 had an effect on the polymerization and dynamics of HpFtsZ. In order to further probe this apparent discrepancy, we analyzed the sequences and molecular structures of FtsZ from various species that included both susceptible and resistant species **(Fig. S4A)**. A detailed structure-based sequence analysis of FtsZ showed that in species that are resistant to PC190723, there are possibly two salt bridges that might play an important role in occluding the inter-domain cleft **(Fig. 8D and Fig. S6)**. The blockage of this cleft might prevent the binding of the drug **(Fig. 8D)**. In species like *E. coli* that are resistant to PC190723, these blockages constitute two salt bridge interactions- Arg307 and Glu198 (shown in red); Asp299 and Arg202 (shown in violet) and one hydrogen bond interaction between the OH group of Ser227 and the main chain of Gly191 (shown in brown) **(Fig. 8D)**. These interactions are absent in *S. aureus* FtsZ; thereby, the drug can be accommodated in the cleft. However, in HpFtsZ, the equivalent position of Glu198 in EcFtsZ is threonine (Thr216), which is smaller than glutamic acid (Glu) and probably far off to engage in any interaction with Arg326 (the equivalent of Arg307 in EcFtsZ) **(Fig. 8E)**. Thus, the salt bridge which might block the drug from binding at the cleft is not present in HpFtsZ **(Fig. 8E)**, thereby possibly allowing PC190723 to bind.

Therefore, restoring the salt-bridge interactions between the amino acids at positions 326 and 216 in HpFtsZ should render it insensitive to PC190723. In order to test this hypothesis, we changed Thr216 in HpFtsZ to glutamic acid (Glu), expressed the mutant HpFtsZ^{T216E} in fission yeast and tested the effect of PC190723 on this mutation. In accordance with the structural analysis, we found no significant difference in the number of

cells having FtsZ polymers in the mutant HpFtsZ^{T216E} upon treatment with PC190723 **(Fig. 7 A and D)**. In the presence or absence of PC190723, HpFtsZ^{T216E} expressing cells showed 47 ± 3.4 % (95% CI; N = 3; 500 cells were counted for each replicate) and 48 ± 14.8 % (95% CI; N = 3; 500 cells were counted for each replicate) respectively, that assembled FtsZ polymers **(Fig. 7A)**. This was unlike HpFtsZ^{WT} **(Fig. 7A and 5C),** where almost 70 % of the cells treated with PC190723 contained polymers as compared to a mere 38 % in untreated cells **(Fig. 7A and 5C)**. The effect size for HpFtsZ^{WT} treated with PC190723 was 28.2 [95% CI 19.8, 36.7] as compared to the effect size for HpFtsZ^{T216E} treated with PC190723, which was 0.9 [95% CI -9.6, 11.5] with a negative value for the lower bound of the confidence interval. Further, like HpFtsZ^{G213A}, HpFtsZ^{T216E} was capable of polymerization and assembled into polymers upon expression in fission yeast **(Fig. S5C)**. Our results here, therefore, suggest that the salt-bridge interactions between residues in H7 helix and adjacent sheets (S7, S9 and S10) in the inter-domain cleft form the basis for the inability of FtsZ in many species to bind to PC190723 rather than a single residue (Arg or His) at position 307 (EcFtsZ).

Discussion

FtsZ is a primary target for the discovery of new antibiotics that inhibit bacterial cell division (Carro, 2019; Schaffner-
Barbero et al., 2012; Silber et al., 2020; Wang et al., 2003). In this study, we have attempted to develop a single step cell-based assay using the fission yeast (*S. pombe*) as the heterologous expression host, which would enable screening of compounds that could directly affect FtsZ polymerization as well as identify those that are toxic to eukaryotic cells in a single step. As a proof-of-principle, we first assessed the ability of FtsZ from two pathogenic species, *S. aureus* and *H. pylori,* to assemble into structures in fission yeast and tested the effects of known FtsZ modulators, sanguinarine, berberine and PC190723

on these FtsZ assemblies. We show that both SaFtsZ and HpFtsZ assembled into structures in fission yeast. While SaFtsZ assembled into spots/ patches or ring-like structures, HpFtsZ assembled into spiral polymers and cables. Although ring-like structures of EcFtsZ have been earlier visualized by confocal laser scanning microscopy (Srinivasan et al., 2008), super-resolution microscopy (SIM) was required to reveal ring-like assemblies in SaFtsZ, suggesting that SaFtsZ likely assembled with a much smaller diameter than EcFtsZ in yeast cells. Interestingly, spiral filaments of FtsZ polymers of *H. pylori* have also been reported in bacterial cells and when expressed in *Drosophila melanogaster* S2 Schneider cells (Specht et al., 2013) suggesting that assembly into helical filaments might be intrinsic to HpFtsZ polymers.

Our results on the ability of sanguinarine and berberine to specifically affect the assembly of FtsZ and not MreB in fission yeast highlight the utility of the heterologous expression system as a platform to identify molecules that specifically affect FtsZ polymerization. Surprisingly, while sanguinarine is known to affect the eukaryotic microtubules (Lopus and Panda, 2006; Wang et al., 2016), we did not observe any significant morphological effects on yeast cells, at least at the lower concentrations of 50 μM used here that affected FtsZ polymerization. However, the drastic morphological defects induced by these drugs at higher concentrations on the yeast cells suggest that they affect the eukaryotic cell physiology. Much higher concentrations of drugs than normally used for mammalian cell cultures have to be used for fission yeast, probably due to permeability issues because of its thick cell wall (Benko et al., 2017). A similar effect of toxicity might arise at lower concentrations in other eukaryotic cells. The permeability of drugs in yeast cells also represents an important caveat in using such heterologous expression systems for the screening of compounds against target molecules. However, notwithstanding this caveat, the heterologous system provides significant advantages in assessing the direct effects of the drug on FtsZ assembly and discerning the toxic effects

of the drug, if any, in eukaryotic cells. Taken together, these results show that while sanguinarine and berberine might affect FtsZ assembly, they are also likely to affect the eukaryotic host cells adversely. This aspect also emphasizes the benefit of utilizing an economic eukaryotic heterologous host for testing drugs targeting bacterial proteins. Any compound that potentially affects eukaryotic function can be easily identified and discarded at the screening step, thus cutting time and costs on further pharmacological analysis in the drug development pipeline.

PC190723 has been one of the most promising drugs against FtsZ and remains the only drug for which the binding site in FtsZ has been clearly established. However, PC190723 predominantly affects Gram +ve bacteria and FtsZ from Gram –ve bacteria have been shown or predicted to be resistant (Haydon et al., 2008). Studies in the past on the effects of PC190723 on *E. coli* have been confusing, with a few reports suggesting an effect on FtsZ polymerization resulting in cell filamentation (Kaul et al., 2014), while others did not find any effect on EcFtsZ
(Anderson et al., 2012; Andreu et al., 2010; Khare et al., 2019). The outer membrane has been shown to be a permeability barrier for PC190723 in *E. coli*
(Chai et al., 2020; Khare et al., 2019). In addition, the Resistance-Nodulation-Division (RND) family of efflux pumps has been attributed to resistance against 2,6-difluorobenzamide derivatives, including TX436 (a prodrug of PC190723) in Gram -ve bacteria (Kaul et al., 2014).

It was, therefore, of interest to test the effects of PC190723 on FtsZ assembly in the yeast expression system, wherein the interpretations are not affected by the compounding factors such as differential membrane permeability or efflux pumps. Our assay provides for a direct comparison of the effect of PC190723 on FtsZ from different species. While our results presented here clearly suggest that PC190723 does not affect the assembly of EcFtsZ, it exerted an effect on HpFtsZ, which is also from a Gram -ve bacterium.

Assemblies of SaFtsZ and HpFtsZ structures appeared in fission yeast cells at a much earlier time when treated with PC190723, suggesting that the drug acted to lower the critical concentration of FtsZ polymerization. Further, FRAP experiments performed on SaFtsZ and HpFtsZ suggest that PC190723 affects the dynamics of FtsZ polymers and slows down the turnover rates. We had earlier shown that FtsZ mutants defective in GTP hydrolysis expressed in fission yeast have slower turnover rates, as measured by fluorescence recovery half-times ($t_{1/2}$) rates (Srinivasan et al., 2008).- These results are also consistent with the earlier findings that PC190723 acts to induce FtsZ polymerization and stabilize FtsZ filaments
(Andreu et al., 2010; Elsen et al., 2012; Fujita et al., 2017; Miguel et al., 2015), and its derivative compound, 8j acting to slow down FtsZ-ring turnover by 3-fold in *B. subtilis* (Adams et al., 2011).

Finally, our studies here suggest that resistance to PC190723 in FtsZ from Gram –ve bacteria like *E. coli* is a result of occluding salt-bridge interactions in the inter-domain cleft between the H7 helix and adjacent sheets (S7, S9 and S10) and may not be due to a single residue (Arg or His) at position 307. Although HpFtsZ contains an arginine at the equivalent position (Arg326), this residue cannot engage in a salt-bridge since HpFtsZ has a threonine (Thr) at position 216 (the equivalent of Glu198 in EcFtsZ). Restoring the salt-bridge interaction in HpFtsZ by changing Thr216 to glutamate (E) conferred resistance to PC190723 in our yeast expression studies. However, PC190723 failed to exert growth inhibition of *H. pylori,* probably owing to outer membrane permeability barriers. Thus, although further genetic, cell biological and biochemical studies will be required to fully elucidate the resistance of *H. pylori* cells to PC190723, our studies here provide new insights into the molecular determinants in FtsZ that lead to resistance against PC190723.

In summary, in this report, we demonstrate the usefulness of the heterologous expression system *S. pombe* for the study of bacterial cytoskeleton-drug interactions. The novelty of this approach lies in the fact that it eliminates any compound that might be toxic to eukaryotic cells at the very first stage and takes a cell-based approach rather than traditional *in-vitro* biochemical screening, which has a poor overall record in antimicrobial discovery. Our results presented here, taken together with the yeast expression studies, suggest that PC190723 could potentially target *H. pylori* FtsZ, and its more permeable derivatives in the future could possibly be a viable therapeutic. However, further *in vivo* studies on FtsZ localization and Z-ring dynamics in *H. pylori* and *in vitro* biochemical studies should provide more insights and ascertain the effect of PC190723 on HpFtsZ. Thus, our results here show that the fission yeast expression system can be used to identify small molecules that directly target FtsZ, probe the molecular determinants of resistance and establish a proof-of-concept of a single step *in vivo* cell-based assay to discover antimicrobials that specifically target the bacterial cytoskeleton.

MATERIALS AND METHODS:

Growth and culture of bacteria and yeast:

The strains and plasmids used in this study are listed in **Supplementary Table S1**. *E. coli* strains and *S. aureus* (ATCC 25923) were grown in LB medium at 37°C, whereas *H. pylori* (strain *H. pylori* 26695) was grown in Brucella broth with 10 % fetal bovine serum media at 37°C with 10 % CO_2. *E. coli* cultures carrying plasmids were grown in LB medium containing appropriate antibiotics (carbenicillin at 100 μg/ mL; kanamycin at 50 μg/ mL; chloramphenicol at 34 μg/ mL). *S. pombe* strain 192 (*h− leu1-32 ura4-D18*) was grown at 30°C in YES medium. Transformation of *S. pombe* was carried out using the Lithium acetate method as described previously (Bähler et al., 1998) and plated on selective Edinburg minimal medium (EMM) plates containing 15 μM thiamine. EMM plates and

broth were supplemented, with adenine (0.225 mg/ mL of media), histidine (0.225 mg/ mL) and leucine (0.225 mg/ mL) or uracil (0.1125 mg/ mL) as necessary. Thiamine was used at a final concentration of 15 μM on the agar plates to repress expression from the medium strength pREP41/42 plasmids. All experiments were done with *S. pombe* growing at 30°C in exponential phase (OD_{600} of 0.3 – 0.6) and were maintained thus by intermittent dilution of cultures. Drugs PC190723, sanguinarine, berberine and A22 were dissolved in DMSO and added to *S. pombe* cultures at a final concentration of 56 μM (20 μg/ mL), 50 μM (18 μg/ mL), 53 μM (20 μg/ mL) and 73.64 μM (20 μg/ mL), respectively with constant shaking or as indicated otherwise in the text or figure legends.

Plasmids and constructs:

Cloning of EcFtsZ, HpFtsZ & SaFtsZ into yeast expression vector pREP42:

EcFtsZ, SaFtsZ and HpFtsZ refer to FtsZ from *E. coli*, *S. aureus* and *H. pylori* respectively. The cloning of EcFtsZ-GFP (pCCD4) into pREP42 has been described previously (Srinivasan et al., 2008). Genomic DNA was isolated from *H. pylori* and *S. aureus* wild-type strains using the Genomic DNA Isolation kit. These genomic DNA were used as a template in a PCR reaction using high-fidelity Q5 polymerase to amplify the *ftsZ* genes of these bacteria. The plasmids pCCD712 and pCCD713 expressing *H. pylori* FtsZ-GFP (HpFtsZ-GFP) and *S. aureus* FtsZ-GFP (SaFtsZ-GFP), respectively, were constructed by cloning the amplified PCR product into pCCD51 using restriction-free (RF) cloning method (van den Ent and Löwe, 2006). pCCD51 was constructed as follows: GFP was amplified by PCR from pCCD4 using oligonucleotides RSO73 and RSO74. The PCR product was subsequently digested with SmaI and ligated into pREP42 (Moreno et al., 2000) linearized with the same enzyme. Site-directed mutagenesis was carried out following the Stratagene™ Quickchange-II site-directed mutagenesis procedure using high-fidelity Q5 polymerase. The oligonucleotides used are listed in **Supplementary Table S2,** and the

list of chemical reagents with their catalogue numbers is listed in **Supplementary Table S3**.

Microscopy and Fluorescence Recovery after Photobleaching:

For imaging, the cells were mounted onto 1.7% or 2% agarose pads containing media in cavity slides and covered with a coverslip No. 1.5 prior to sealing with VALAP (1:1:1 mixture of vaseline, lanolin and paraffin). Images were acquired using an epifluorescence microscope (DeltaVision™ Elite) with a 100 X oil immersion objective lens of NA 1.4 and equipped with a Photometrics CoolSNAP™ HQ2 camera. An oil of refractive index 1.516 was used for imaging yeasts. Excitation filters and emission filters of 475/28 nm and 525/48 nm were used to image GFP. Z-stacks were acquired with a Z-depth of 0.2 or 0.3 µm. SoftWorX™ software was used to perform deconvolution using the iterative-constrained algorithm (Agard, 1984) with the number of cycles set to 10 (ten). FRAP experiments were carried out essentially as described before (Recovery half-times were calculated as described previously (Anderson et al., 2004; Srinivasan et al., 2008) except that a DeltaVision™ equipped with a Quantitative laser module (QLM; X4 Laser) was used for imaging. Photobleaching was carried out using 80% laser power with an argon laser (488 nm) with a pulse time of 0.05 sec. Images were acquired before and after photobleaching, and Z-stack images were acquired at fixed intervals with a Z-depth of 0.2 or 0.3 µm. Time-lapse intervals were varied or were typically 1 – 2 seconds apart and acquired for over 2 minutes. Integrated fluorescence intensities in the pre-bleached images and at each time point in the bleached and other regions were measured in Fiji (v 2.0.0-rc-69/1.52p). FRAP experiments were performed on different days, and data were pooled for analysis. All values were exported to Excel (Microsoft™) for further analysis. The recovery half-time ($t_{1/2}$) values mentioned in the text were obtained by fitting the fluorescence recovery curves to a single exponential curve $F(t)= C(1 - e^{-kt})$ and

calculated from $t_{1/2} = \ln(2)/k$. The solver function in Excel was used for the least-squares fit of the corrected fluorescence intensities over time to the single exponential equation. All images were processed using Fiji (v 2.0.0-rc-69/1.52p) (Schindelin et al., 2012).

Sequence and structural analysis for PC190723 binding to FtsZ

The sequences of FtsZs from various organisms were taken from UniProt, aligned using Clustal Omega (Sievers et al., 2011), and represented using Jalview (Waterhouse et al., 2009). The reference structure taken for the analysis was the previously reported T state structure of SaFtsZ bound to PC190723 (PDB ID: 4DXD), and the residues around 4 Å were determined using UCSF Chimera version 1.13.1 (Pettersen et al., 2004). The residues in SaFtsZ, which contributed to the binding of the drug, were highlighted in the sequence alignment. The reference R state structure (PDB ID: 5H5I) was chosen to see whether the drug can be accommodated in the R state structure of SaFtsZ by superimposing the C- alpha atoms of the nucleotide-binding domain (NBD) of 5H5I and 4DXD. FtsZs from *H. pylori* and *E.coli* were modelled in T state using SWISS-MODEL (Waterhouse et al., 2018), with PDB ID 4DXD as the template. Similarly, the NBD of the modelled structures was superimposed onto the SaFtsZ structure bound to PC190723 and checked whether the drug could be accommodated in the corresponding pocket of the models without significant clashes.

Statistical Analysis

All statistical analysis and tests were carried out in Excel (Office 365 or Excel for Mac 2011) using the built-in Data Analysis functions or the add-ins XLSTAT or Xrealstat (Real Statistics). A single colony of bacteria or a patch of yeast cells independently grown from freshly streaked out cells on agar plates from frozen glycerol stocks was considered to be

a biological replicate. A minimum of at least 3 biological replicates was used for every experiment. The dosage effect upon increasing concentrations of PC190723 on FtsZ assembly was assessed using the Cochran-Armitage test. A two-proportions z-test was used for the statistical analysis of the effect of PC190723 on the proportions of cells carrying FtsZ polymers and the calculation of P-values. An unpaired two-sided Student's t-test was used as a statistical test for the FRAP experiments. Statistical tests and P-values are indicated in the figure legends using an asterisk. A P-value ≤ 0.0001, ≤ 0.001, ≤ 0.01, , ≤ 0.05 or > 0.05 indicated by ****, ***, **, * and ns respectively. As an alternative to null-hypothesis significance tests (NHST), we also used estimation statistics to determine the effect size and 95 % confidence intervals (Claridge-Chang and Assam, 2016; Ho et al., 2019). The error bars plotted are inferential and represent the 95% CI (Cumming et al., 2007; Pollard et al., 2019; Vaux, 2014).

Acknowledgement

The authors thank Prof. Jose Manuel Andreu and Dr. Lidia Araujo-Bazán for their critical reading of the article and valuable comments and suggestions. The authors are grateful to Dr. Asima Bhattacharyya (SBS, NISER, India) for *H. pylori* genomic DNA and Dr. Mithilesh Mishra (DBS, TIFR, Mumbai, India) for strains and plasmids. This work is supported by the Department of Biotechnology (DBT) from BT/PR15183/BRB/10/1443/2015 to RS and BT/PR42977/BRB/10/2022/2021 to RS & GP and DBT Membrane Structural Biology Program grant - BT/PR28833/BRB/10/1705/2018 to PG. PG also acknowledges support from INSPIRE Faculty Fellowship from (IFA12/LSBM-52), Department of Science and Technology, and Innovative Young Biotechnologist Award (BT/07/IYBA/2013). Intramural core funding from the Department of Atomic Energy (DAE) and support staff members at the Centre of Interdisciplinary Sciences, NISER, are acknowledged. We also

acknowledge fellowships from DAE to AKS, SMP, BSN, SK, NM and from IISER Pune to JC.

Author contributions:

AKS, SMP, BSN conducted the experiments. RS, GP and JC designed and analyzed the work. BSN initiated the work, SMP contributed to initial optimization, and AKS optimized further and carried out the experiments. AKS carried out the analysis and quantification of the data. SMP carried out the work related to the MIC and resistance mutants. JC carried out all the *in silico* work and structural analysis. AKS, JC, GP and RS wrote the manuscript. AKS, SMP and JC edited the draft manuscripts. SK contributed to the plotting and analysis of FRAP data. NM carried out the experiments related to MreB and A22 treatment.

References

Bibliography

Adams, D.W., Wu, L.J., Czaplewski, L.G., and Errington, J. (2011). Multiple effects of benzamide antibiotics on FtsZ function. Mol. Microbiol. *80*, 68–84.

Adams, D.W., Wu, L.J., and Errington, J. (2016). A benzamide-dependent ftsZ mutant reveals residues crucial for Z-ring assembly. Mol. Microbiol. *99*, 1028–1042.

Addinall, S.G., and Holland, B. (2002). The tubulin ancestor, FtsZ, draughtsman, designer and driving force for bacterial cytokinesis. J. Mol. Biol. *318*, 219–236.

Addinall, S.G., and Lutkenhaus, J. (1996). FtsZ-spirals and -arcs determine the shape of the invaginating septa in some mutants of Escherichia coli. Mol. Microbiol. *22*, 231–237.

Agard, D. (1984). Optical sectioning microscopy: cellular architecture in three dimensions. Annu. Rev. Biophys. Biomol. Struct. *13*, 191–219.

Anderson, D.E., Gueiros-Filho, F.J., and Erickson, H.P. (2004). Assembly dynamics of FtsZ rings in Bacillus subtilis and Escherichia coli and effects of FtsZ-regulating proteins. J. Bacteriol. *186*, 5775–5781.

Anderson, D.E., Kim, M.B., Moore, J.T., O'Brien, T.E., Sorto, N.A., Grove, C.I., Lackner, L.L., Ames, J.B., and Shaw, J.T. (2012). Comparison of small molecule inhibitors of the bacterial cell division protein FtsZ and identification of a reliable cross-species inhibitor. ACS Chem. Biol. *7*, 1918–1928.

Andreu, J.M., Schaffner-Barbero, C., Huecas, S., Alonso, D., Lopez-Rodriguez, M.L., Ruiz-Avila, L.B., Núñez-Ramírez, R., Llorca, O., and Martín-Galiano, A.J. (2010). The antibacterial cell division inhibitor PC190723 is an FtsZ polymer-stabilizing agent that induces filament assembly and condensation. J. Biol. Chem. *285*, 14239–14246.

Bähler, J., Wu, J.-Q., Longtine, M.S., Shah, N.G., Mckenzie III, A., Steever, A.B., Wach, A., Philippsen, P., and Pringle, J.R. (1998). Heterologous modules for efficient and versatile PCR-based gene targeting in *Schizosaccharomyces pombe*. Yeast *14*, 943–951.

Barrows, J.M., and Goley, E.D. (2021). FtsZ dynamics in bacterial division: What, how, and why? Curr. Opin. Cell Biol. *68*, 163–172.

Basi, G., Schmid, E., and Maundrell, K. (1993). TATA box mutations in the Schizosaccharomyces pombe nmt1 promoter affect transcription efficiency but not the transcription start point or thiamine repressibility. Gene *123*, 131–136.

Benko, Z., Liang, D., Li, G., Elder, R.T., Sarkar, A., Takayama, J., Ghosh, A.K., and Zhao, R.Y. (2017). A fission yeast cell-based system for multidrug resistant HIV-1 proteases. Cell Biosci. *7*, 5.

Beuria, T.K., Santra, M.K., and Panda, D. (2005). Sanguinarine blocks cytokinesis in bacteria by inhibiting FtsZ assembly and bundling. Biochemistry *44*, 16584–16593.

Bi, E.F., and Lutkenhaus, J. (1991). FtsZ ring structure associated with division in Escherichia coli. Nature *354*, 161–164.

Boberek, J.M., Stach, J., and Good, L. (2010). Genetic evidence for inhibition of bacterial division protein FtsZ by berberine. PLoS ONE *5*, e13745.

Bramhill, D., and Thompson, C.M. (1994). GTP-dependent polymerization of Escherichia coli FtsZ protein to form tubules. Proc Natl Acad Sci USA *91*, 5813–5817.

Butler, M.S., and Paterson, D.L. (2020). Antibiotics in the clinical pipeline in October 2019. J. Antibiot. *73*, 329–364.

Carro, L. (2019). Recent Progress in the Development of Small-Molecule FtsZ Inhibitors as Chemical Tools for the Development of Novel Antibiotics. Antibiotics (Basel) *8*.

Chai, W.C., Whittall, J.J., Song, D., Polyak, S.W., Ogunniyi, A.D., Wang, Y., Bi, F., Ma, S., Semple, S.J., and Venter, H. (2020). Antimicrobial action and reversal of resistance in MRSA by difluorobenzamide derivatives targeted at ftsz. Antibiotics (Basel) *9*.

Claridge-Chang, A., and Assam, P.N. (2016). Estimation statistics should replace significance testing. Nat. Methods *13*, 108–109.

Cumming, G., Fidler, F., and Vaux, D.L. (2007). Error bars in experimental biology. J. Cell Biol. *177*, 7–11.

Domadia, P.N., Bhunia, A., Sivaraman, J., Swarup, S., and Dasgupta, D. (2008). Berberine targets assembly of Escherichia coli cell division protein FtsZ. Biochemistry *47*, 3225–3234.

Elsen, N.L., Lu, J., Parthasarathy, G., Reid, J.C., Sharma, S., Soisson, S.M., and Lumb, K.J. (2012). Mechanism of action of the cell-division inhibitor PC190723: modulation of FtsZ assembly cooperativity. J. Am. Chem. Soc. *134*, 12342–12345.

van den Ent, F., and Löwe, J. (2006). RF cloning: a restriction-free method for inserting target genes into plasmids. J. Biochem. Biophys. Methods *67*, 67–74.

Erickson, H.P. (1995). FtsZ, a prokaryotic homolog of tubulin? Cell *80*, 367–370.

Erickson, H.P., Anderson, D.E., and Osawa, M. (2010). FtsZ in bacterial cytokinesis: cytoskeleton and force generator all in one. Microbiol. Mol. Biol. Rev. *74*, 504–528.

Fujita, J., Maeda, Y., Mizohata, E., Inoue, T., Kaul, M., Parhi, A.K., LaVoie, E.J., Pilch, D.S., and Matsumura, H. (2017). Structural Flexibility of an Inhibitor Overcomes Drug Resistance Mutations in Staphylococcus aureus FtsZ. ACS Chem. Biol. *12*, 1947–1955.

Gitai, Z., Dye, N.A., Reisenauer, A., Wachi, M., and Shapiro, L. (2005). MreB actin-mediated segregation of a specific region of a bacterial chromosome. Cell *120*, 329–341.

Haydon, D.J., Stokes, N.R., Ure, R., Galbraith, G., Bennett, J.M., Brown, D.R., Baker, P.J., Barynin, V.V., Rice, D.W., Sedelnikova, S.E., et al. (2008). An inhibitor of FtsZ with potent and selective anti-staphylococcal activity. Science *321*, 1673–1675.

Ho, J., Tumkaya, T., Aryal, S., Choi, H., and Claridge-Chang, A. (2019). Moving beyond P values: data analysis with estimation graphics. Nat. Methods *16*, 565–566.

Huang, K.-H., Durand-Heredia, J., and Janakiraman, A. (2013). FtsZ ring stability: of bundles, tubules, crosslinks, and curves. J. Bacteriol. *195*, 1859–1868.

Hurley, K.A., Santos, T.M., Nepomuceno, G.M., Huynh, V., Shaw, J.T., and Weibel, D.B. (2016). Targeting the bacterial division protein FtsZ. J. Med. Chem. *59*, 6975–6998.

Iwai, N., Nagai, K., and Wachi, M. (2002). Novel S-benzylisothiourea compound that induces spherical cells in Escherichia coli probably by acting on a rod-shape-determining protein(s) other than penicillin-binding protein 2. Biosci. Biotechnol. Biochem. *66*, 2658–2662.

Kaul, M., Parhi, A.K., Zhang, Y., LaVoie, E.J., Tuske, S., Arnold, E., Kerrigan, J.E., and Pilch, D.S. (2012). A bactericidal guanidinomethyl biaryl that alters the dynamics of bacterial FtsZ polymerization. J. Med. Chem. *55*, 10160–10176.

Kaul, M., Zhang, Y., Parhi, A.K., Lavoie, E.J., Tuske, S., Arnold, E., Kerrigan, J.E., and Pilch, D.S. (2013a). Enterococcal and streptococcal resistance to PC190723 and related compounds: molecular insights from a FtsZ mutational analysis. Biochimie *95*, 1880–1887.

Kaul, M., Mark, L., Zhang, Y., Parhi, A.K., LaVoie, E.J., and Pilch, D.S. (2013b). Pharmacokinetics and in vivo antistaphylococcal efficacy of TXY541, a 1-methylpiperidine-4-carboxamide prodrug of PC190723. Biochem. Pharmacol. *86*, 1699–1707.

Kaul, M., Zhang, Y., Parhi, A.K., Lavoie, E.J., and Pilch, D.S. (2014). Inhibition of RND-type efflux pumps confers the FtsZ-directed prodrug TXY436 with activity against Gram-negative bacteria. Biochem. Pharmacol. *89*, 321–328.

Kelley, C., Zhang, Y., Parhi, A., Kaul, M., Pilch, D.S., and LaVoie, E.J. (2012). 3-Phenyl substituted 6,7-dimethoxyisoquinoline derivatives as FtsZ-targeting antibacterial agents. Bioorg. Med. Chem. *20*, 7012–7029.

Khare, S., Hsin, J., Sorto, N.A., Nepomuceno, G.M., Shaw, J.T., Shi, H., and Huang, K.C. (2019). FtsZ-Independent Mechanism of Division Inhibition by the Small Molecule PC190723 in Escherichia coli. Adv. Biosys. *3*, e1900021.

Kumar, K., Awasthi, D., Lee, S.-Y., Zanardi, I., Ruzsicska, B., Knudson, S., Tonge, P.J., Slayden, R.A., and Ojima, I. (2011). Novel trisubstituted benzimidazoles, targeting Mtb FtsZ, as a new class of antitubercular agents. J. Med. Chem. *54*, 374–381.

Kusuma, K.D., Payne, M., Ung, A.T., Bottomley, A.L., and Harry, E.J. (2019). Ftsz as an antibacterial target: status and guidelines for progressing this avenue. ACS Infect. Dis. *5*, 1279–1294.

Liu, F., Venter, H., Bi, F., Semple, S.J., Liu, J., Jin, C., and Ma, S. (2017). Synthesis and antibacterial activity of 5-methylphenanthridium derivatives as FtsZ inhibitors. Bioorg. Med. Chem. Lett. *27*, 3399–3402.

Lopus, M., and Panda, D. (2006). The benzophenanthridine alkaloid sanguinarine perturbs microtubule assembly dynamics through tubulin binding. A possible mechanism for its antiproliferative activity. FEBS J. *273*, 2139–2150.

Löwe, J., and Amos, L.A. (1998). Crystal structure of the bacterial cell-division protein FtsZ. Nature *391*, 203–206.

Mahone, C.R., and Goley, E.D. (2020). Bacterial cell division at a glance. J. Cell Sci. *133*.

Margalit, D.N., Romberg, L., Mets, R.B., Hebert, A.M., Mitchison, T.J., Kirschner, M.W., and RayChaudhuri, D. (2004). Targeting cell division: small-molecule inhibitors of FtsZ GTPase perturb cytokinetic ring assembly and induce bacterial lethality. Proc Natl Acad Sci USA *101*, 11821–11826.

Margolin, W. (2005). FtsZ and the division of prokaryotic cells and organelles. Nat. Rev. Mol. Cell Biol. *6*, 862–871.

Matsui, T., Yamane, J., Mogi, N., Yamaguchi, H., Takemoto, H., Yao, M., and Tanaka, I. (2012). Structural reorganization of the bacterial cell-division protein FtsZ from Staphylococcus aureus. Acta Crystallogr. D Biol. Crystallogr. *68*, 1175–1188.

Ma, X., Ehrhardt, D.W., and Margolin, W. (1996). Colocalization of cell division proteins FtsZ and FtsA to cytoskeletal structures in living Escherichia coli cells by using green fluorescent protein. Proc Natl Acad Sci USA *93*, 12998–13003.

Miguel, A., Hsin, J., Liu, T., Tang, G., Altman, R.B., and Huang, K.C. (2015). Variations in the binding pocket of an inhibitor of the bacterial division protein FtsZ across genotypes and species. PLoS Comput. Biol. *11*, e1004117.

Moreno, M.B., Durán, A., and Carlos Ribas, J. (2000). A family of multifunctional thiamine-repressible expression vectors for fission yeast. Yeast *16*, 861–872.

Nogales, E., Downing, K.H., Amos, L.A., and Löwe, J. (1998). Tubulin and FtsZ form a distinct family of GTPases. Nat. Struct. Biol. *5*, 451–458.

Obiang-Obounou, B.W., Kang, O.-H., Choi, J.-G., Keum, J.-H., Kim, S.-B., Mun, S.-H., Shin, D.-W., Kim, K.W., Park, C.-B., Kim, Y.-G., et al. (2011). The mechanism of action of sanguinarine against methicillin-resistant Staphylococcus aureus. J. Toxicol. Sci. *36*, 277–283.

Pettersen, E.F., Goddard, T.D., Huang, C.C., Couch, G.S., Greenblatt, D.M., Meng, E.C., and Ferrin, T.E. (2004). UCSF Chimera—a visualization system for exploratory research and analysis. J. Comput. Chem. *25*, 1605–1612.

Pollard, D.A., Pollard, T.D., and Pollard, K.S. (2019). Empowering statistical methods for cellular and molecular biologists. Mol. Biol. Cell *30*, 1359–1368.

Pradhan, P., Margolin, W., and Beuria, T.K. (2021). Targeting the achilles heel of ftsz: the interdomain cleft. Front. Microbiol. *12*, 732796.

RayChaudhuri, D., and Park, J.T. (1992). Escherichia coli cell-division gene ftsZ encodes a novel GTP-binding protein. Nature *359*, 251–254.

Schaffner-Barbero, C., Martín-Fontecha, M., Chacón, P., and Andreu, J.M. (2012). Targeting the assembly of bacterial cell division protein FtsZ with small molecules. ACS Chem. Biol. *7*, 269–277.

Schindelin, J., Arganda-Carreras, I., Frise, E., Kaynig, V., Longair, M., Pietzsch, T., Preibisch, S., Rueden, C., Saalfeld, S., Schmid, B., et al. (2012). Fiji: an open-source platform for biological-image analysis. Nat. Methods *9*, 676–682.

Sievers, F., Wilm, A., Dineen, D., Gibson, T.J., Karplus, K., Li, W., Lopez, R., McWilliam, H., Remmert, M., Söding, J., et al. (2011). Fast, scalable generation of high-quality protein multiple sequence alignments using Clustal Omega. Mol. Syst. Biol. *7*, 539.

Silber, N., Matos de Opitz, C.L., Mayer, C., and Sass, P. (2020). Cell division protein FtsZ: from structure and mechanism to antibiotic target. Future Microbiol. *15*, 801–831.

Specht, M., Dempwolff, F., Schätzle, S., Thomann, R., and Waidner, B. (2013). Localization of FtsZ in Helicobacter pylori and consequences for cell division. J. Bacteriol. *195*, 1411–1420.

Srinivasan, R., Mishra, M., Murata-Hori, M., and Balasubramanian, M.K. (2007). Filament formation of the Escherichia coli actin-related protein, MreB, in fission yeast. Curr. Biol. *17*, 266–272.

Srinivasan, R., Mishra, M., Wu, L., Yin, Z., and Balasubramanian, M.K. (2008). The bacterial cell division protein FtsZ assembles into cytoplasmic rings in fission yeast. Genes Dev. *22*, 1741–1746.

Stokes, N.R., Baker, N., Bennett, J.M., Berry, J., Collins, I., Czaplewski, L.G., Logan, A., Macdonald, R., Macleod, L., Peasley, H., et al. (2013). An improved small-molecule inhibitor of FtsZ with superior in vitro potency, drug-like properties, and in vivo efficacy. Antimicrob. Agents Chemother. *57*, 317–325.

Straniero, V., Zanotto, C., Straniero, L., Casiraghi, A., Duga, S., Radaelli, A., De Giuli Morghen, C., and Valoti, E. (2017). 2,6-Difluorobenzamide Inhibitors of Bacterial Cell Division Protein FtsZ: Design, Synthesis, and Structure-Activity Relationships. ChemMedChem *12*, 1303–1318.

Straniero, V., Sebastián-Pérez, V., Hrast, M., Zanotto, C., Casiraghi, A., Suigo, L., Zdovc, I., Radaelli, A., De Giuli Morghen, C., and Valoti, E. (2020). Benzodioxane-Benzamides as Antibacterial Agents: Computational and SAR Studies to Evaluate the Influence of the 7-Substitution in FtsZ Interaction. ChemMedChem *15*, 195–209.

Sun, N., Chan, F.-Y., Lu, Y.-J., Neves, M.A.C., Lui, H.-K., Wang, Y., Chow, K.-Y., Chan, K.-F., Yan, S.-C., Leung, Y.-C., et al. (2014). Rational design of berberine-based FtsZ inhibitors with broad-spectrum antibacterial activity. PLoS ONE *9*, e97514.

Tan, C.M., Therien, A.G., Lu, J., Lee, S.H., Caron, A., Gill, C.J., Lebeau-Jacob, C., Benton-Perdomo, L., Monteiro, J.M., Pereira, P.M., et al. (2012). Restoring methicillin-

resistant Staphylococcus aureus susceptibility to β-lactam antibiotics. Sci. Transl. Med. *4*, 126ra35.

TAXIS Pharmaceuticals (2020). TAXIS secures NIH Funding – TAXIS Pharmaceutical.

Vaughan, S., Wickstead, B., Gull, K., and Addinall, S.G. (2004). Molecular evolution of FtsZ protein sequences encoded within the genomes of archaea, bacteria, and eukaryota. J. Mol. Evol. *58*, 19–29.

Vaux, D.L. (2014). Basic statistics in cell biology. Annu. Rev. Cell Dev. Biol. *30*, 23–37.

Vollmer, W. (2006). The prokaryotic cytoskeleton: a putative target for inhibitors and antibiotics? Appl. Microbiol. Biotechnol. *73*, 37–47.

Wang, J., Galgoci, A., Kodali, S., Herath, K.B., Jayasuriya, H., Dorso, K., Vicente, F., González, A., Cully, D., Bramhill, D., et al. (2003). Discovery of a small molecule that inhibits cell division by blocking FtsZ, a novel therapeutic target of antibiotics. J. Biol. Chem. *278*, 44424–44428.

Wang, X., Tanaka, M., Krstin, S., Peixoto, H.S., and Wink, M. (2016). The Interference of Selected Cytotoxic Alkaloids with the Cytoskeleton: An Insight into Their Modes of Action. Molecules *21*.

Waterhouse, A.M., Procter, J.B., Martin, D.M.A., Clamp, M., and Barton, G.J. (2009). Jalview Version 2--a multiple sequence alignment editor and analysis workbench. Bioinformatics *25*, 1189–1191.

Waterhouse, A., Bertoni, M., Bienert, S., Studer, G., Tauriello, G., Gumienny, R., Heer, F.T., de Beer, T.A.P., Rempfer, C., Bordoli, L., et al. (2018). SWISS-MODEL: homology modelling of protein structures and complexes. Nucleic Acids Res. *46*, W296–W303.

Weiss, D.S. (2004). Bacterial cell division and the septal ring. Mol. Microbiol. *54*, 588–597.

Weiss, D.S., Chen, J.C., Ghigo, J.M., Boyd, D., and Beckwith, J. (1999). Localization of FtsI (PBP3) to the septal ring requires its membrane anchor, the Z ring, FtsA, FtsQ, and FtsL. J. Bacteriol. *181*, 508–520.

Zorrilla, S., Monterroso, B., Robles-Ramos, M.-Á., Margolin, W., and Rivas, G. (2021). FtsZ interactions and biomolecular condensates as potential targets for new antibiotics. Antibiotics (Basel) *10*.

Figures

Figure 1

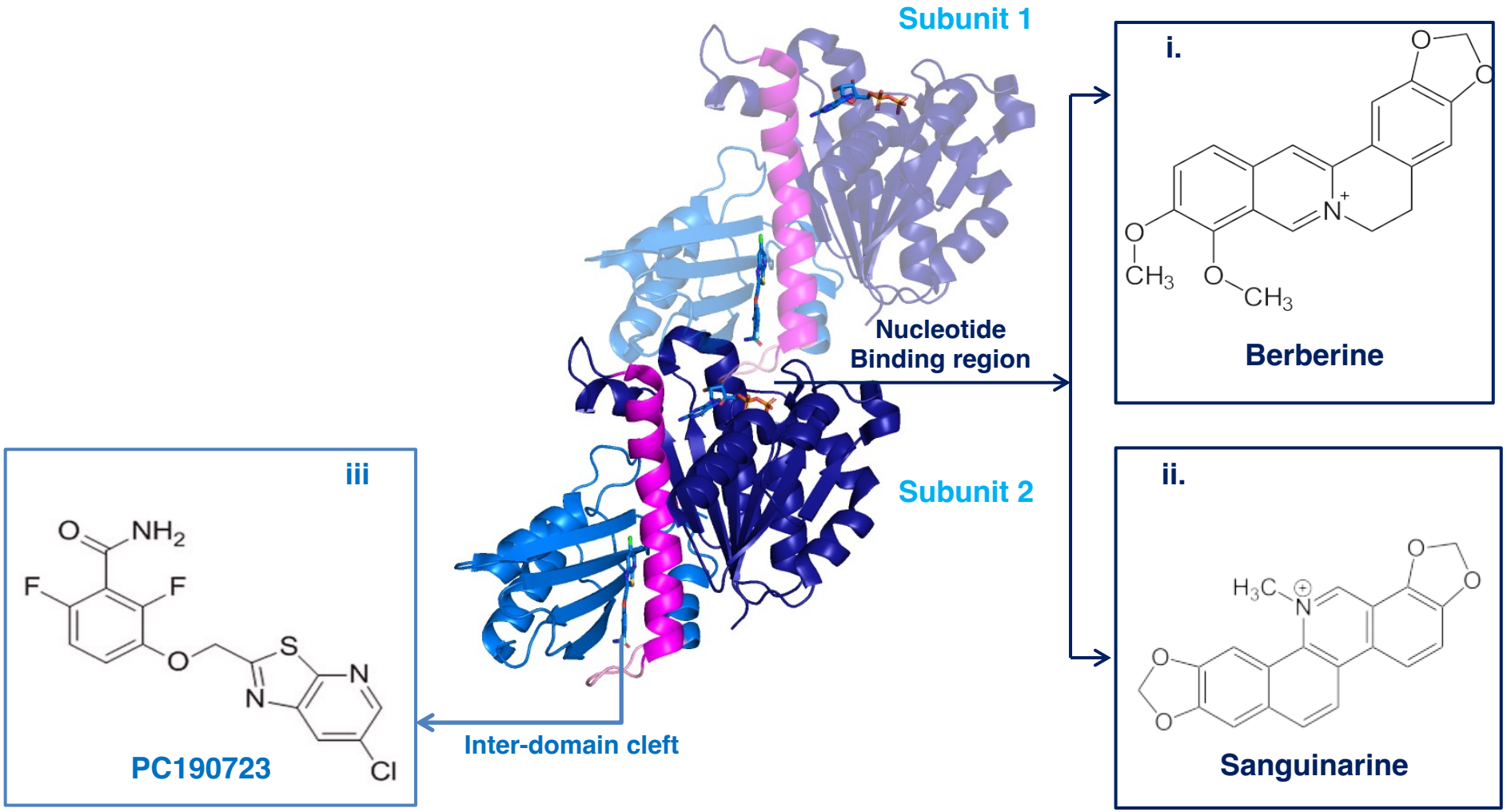
Subunit 1
Nucleotide
Binding region
Subunit 2
Inter-domain cleft
i.
Berberine
ii.
Sanguinarine
iii
PC190723

Figure Legends:

Figure 1. Overall structure of FtsZ showing the binding pockets of known drugs targeted to FtsZ. Overall head to tail structure of SaFtsZ bound to PC190723 (PDB-4DXD; NTD – dark blue, H7 helix and T7 loop – magenta and CTD – blue. The other subunit (top) is shown in partial transparent mode. Binding sites of the drugs known to target FtsZ- **i)** Berberine, a quaternary ammonium base 9,10-dimethoxy-5,6-dihydro[1,3] dioxolo[4,5-g]isoquino[3,2-a]isoquinoline-7-ilium obtained from various species of *Berberis* such as *B. aquifolium* and *B. aristate* (dark blue). **ii)** Sanguinarine, a benzophenanthridine alkaloid [13-methyl-(1,3)-benzodioxolo-(5,6-c)1,3-dioxolo-(4,5-i)phenanthridinium] and is derived from the rhizomes of *Sanguinaria canadensis* (dark blue). and **iii)** PC190723, a synthetic 2,6-difluorinated 3-methoxybenzamide derivative (blue).

Figure 2

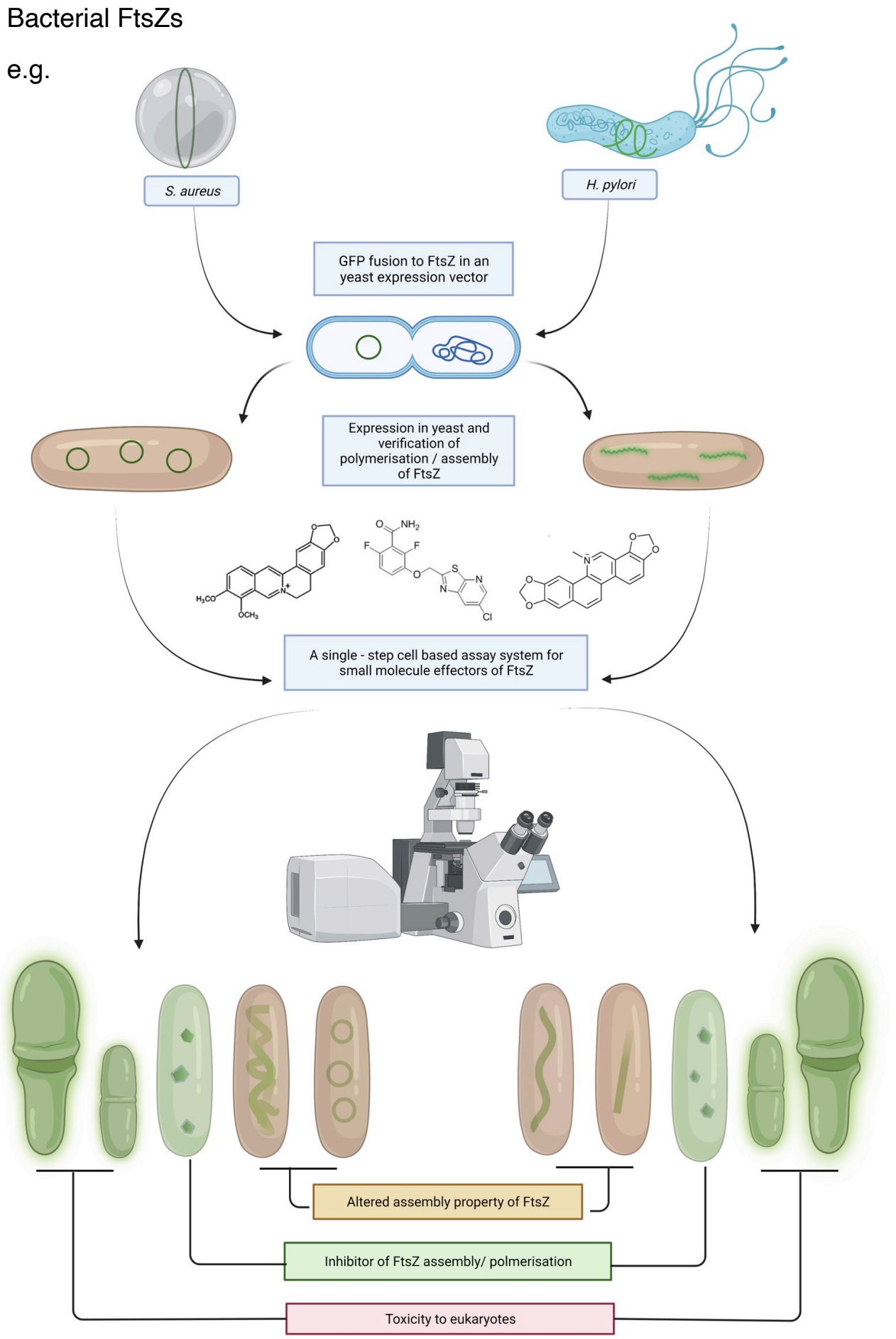
Bacterial FtsZs
e.g.
S. aureus
H. pylori
GFP fusion to FtsZ in an yeast expression vector
Expression in yeast and verification of polymerisation / assembly of FtsZ
A single - step cell based assay system for small molecule effectors of FtsZ
Altered assembly property of FtsZ
Inhibitor of FtsZ assembly/ polmerisation
Toxicity to eukaryotes

Figure 2. Schematic of the single-step cell-based assay to identify direct inhibitors of bacterial cytoskeletal proteins. A GFP-fusion to FtsZ from chosen bacterial species is expressed in yeast cells such as *S. pombe*. Expression and assembly of FtsZ in yeast cells is verified by fluorescence microscopy. Yeast cells are grown in the presence of known small molecules or chemical libraries. Effect of known compounds on FtsZ assembly and dynamics are assessed by imaging. While molecules toxic to the yeast cells are screened by growth or morphological changes, compounds inhibiting or altering the assembly of FtsZ (or the expressed bacterial cytoskeletal protein) are deemed potential hits and further scrutinized.

Figure 3

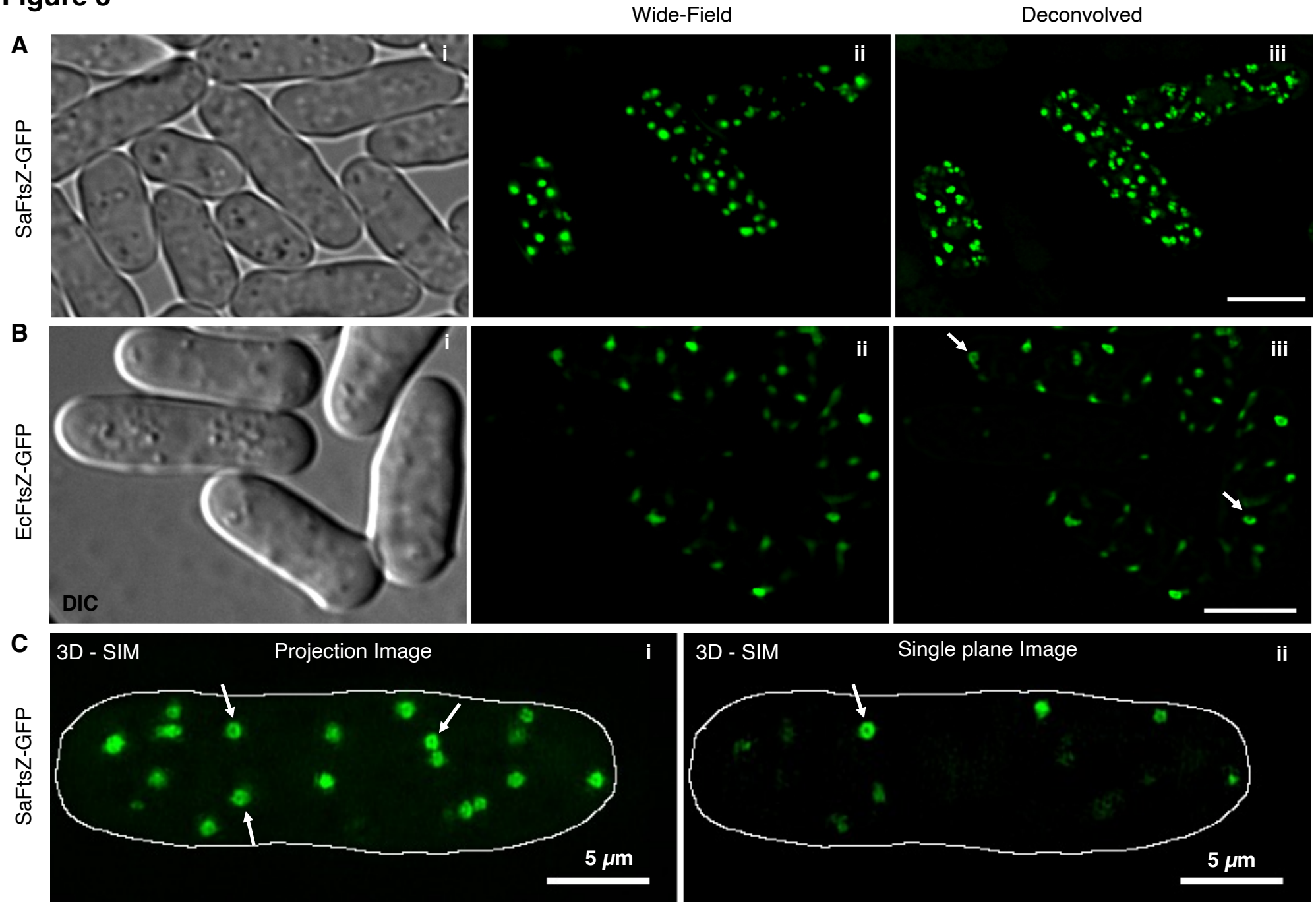
Wide-Field
Deconvolved
A
SaFtsZ-GFP
i
ii
iii
B
EcFtsZ-GFP
i
ii
iii
DIC
C
SaFtsZ-GFP
3D - SIM
Projection Image
i
5 μm
3D - SIM
Single plane Image
ii
5 μm

Figure 3

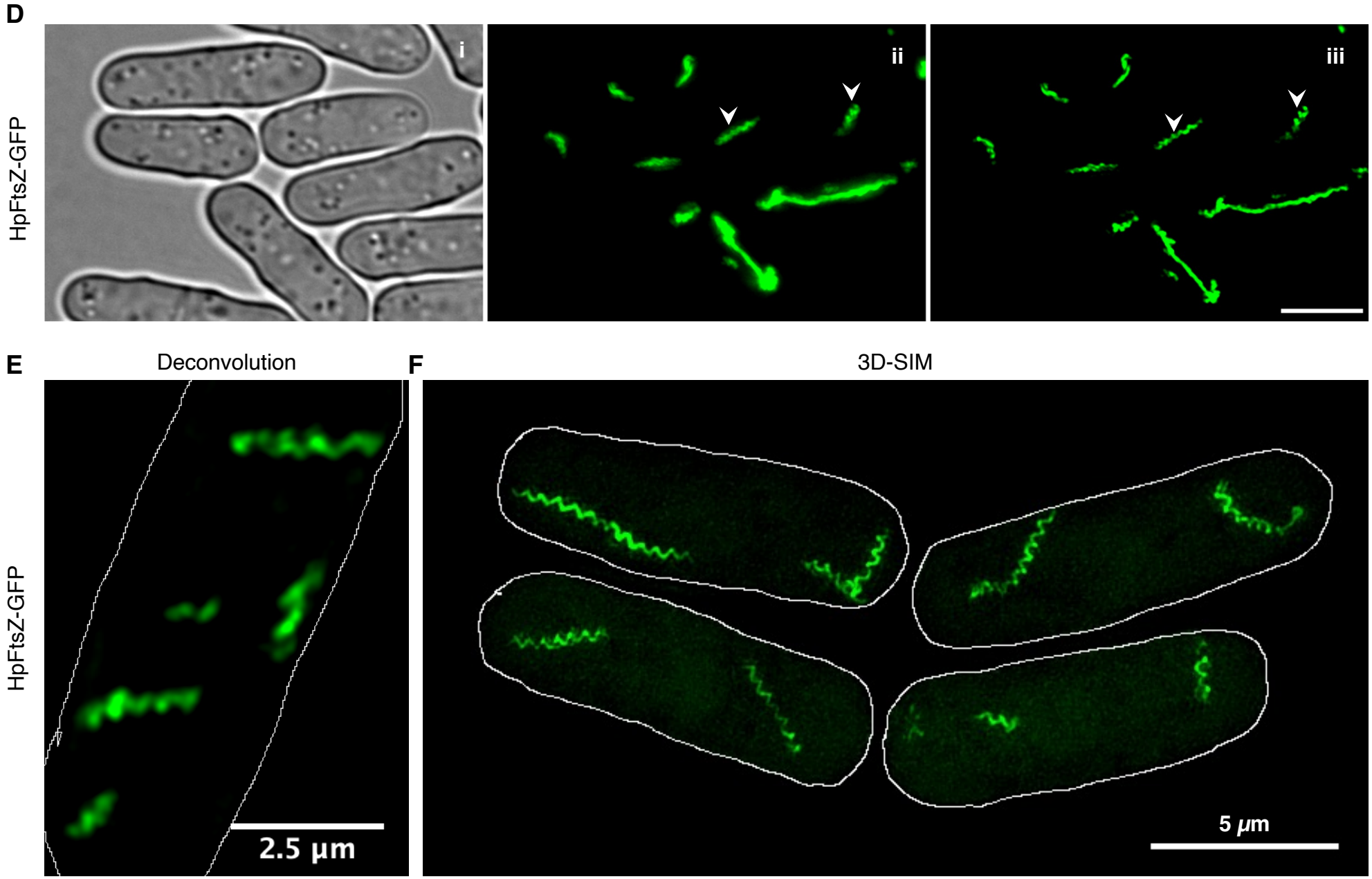
D
HpFtsZ-GFP
i
ii
iii
E
Deconvolution
HpFtsZ-GFP
2.5 µm
F
3D-SIM
5 µm

Figure 3. Polymerisation of SaFtsZ, EcFtsZ and HpFtsZ in fission yeast. The medium-strength *nmt42* promoter was used for the expression of different bacterial FtsZ-GFP fusion constructs in *S. pombe*. *S. pombe* cultures expressing FtsZ-GFP fusions were grown for 16–20 h at 30°C in the absence of thiamine to allow the expression of the proteins, mounted onto 1.6% agarose slide, and imaged using an **(A, B and D)** epifluorescence microscope or **(C and F)** super-resolution using 3D-SIM. **(A)** SaFtsZ and **(B)** EcFtsZ assembles into spots and cable-like structures in fission yeast (panels ii and iii). Arrows indicate ring-like structures. **(C)** 3D-SIM images of SaFtsZ. **(C i)** Maximum intensity projection image and **(C ii)** a single plane image reveal ring-like structures of SaFtsZ. Arrows indicate visible SaFtsZ rings. **(D)** HpFtsZ forms cable-like structures. Helical filaments of HpFtsZ are indicated by arrowheads. DIC or phase-contrast images are shown in **Ai, Bi & Di**. **(E)** Deconvolved image of HpFtsZ and **(F)** 3D-SIM images of HpFtsZ show the assembly of HpFtsZ into helical filaments in fission yeast. Scale bar represents 5 μm for all images **(A – D & F)** except for the image in **E** where it represents 2.5 μm.

Figure 4

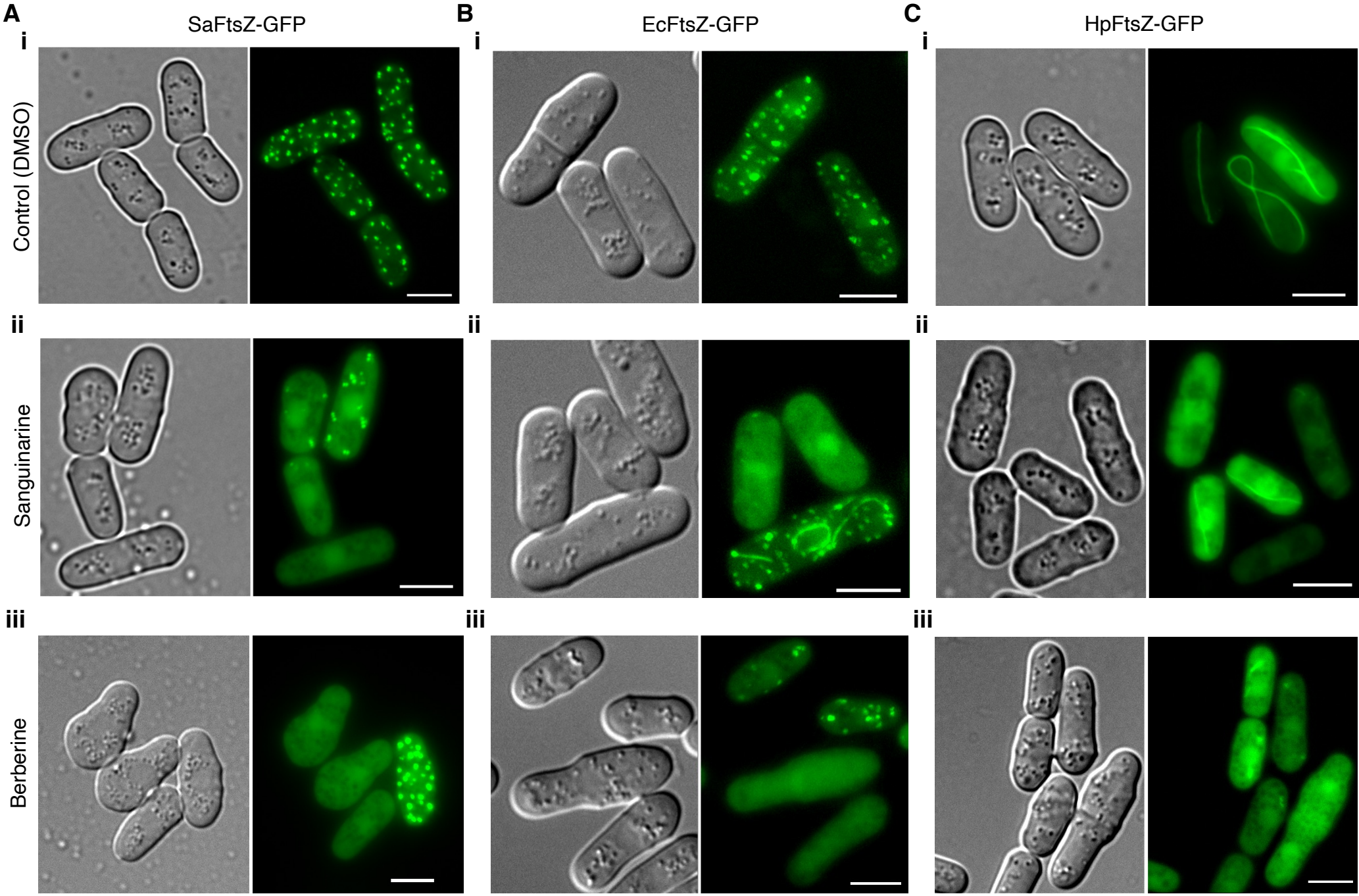
A
SaFtsZ-GFP
B
EcFtsZ-GFP
C
HpFtsZ-GFP
i
ii
iii
Control (DMSO)
Sanguinarine
Berberine

Figure 4

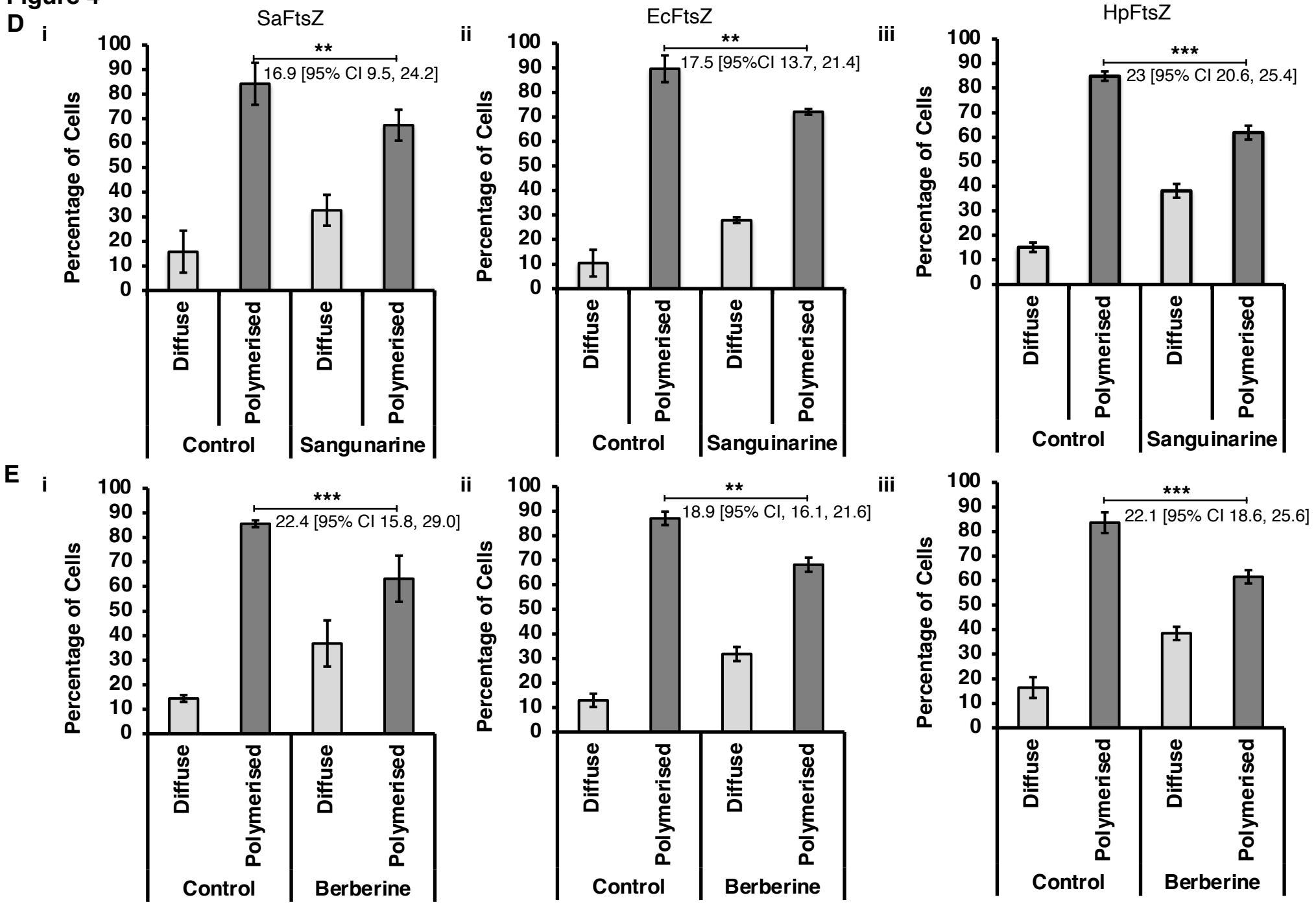
D
i
SaFtsZ
Percentage of Cells
100
90
80
70
60
50
40
30
20
10
0
**
16.9 [95% CI 9.5, 24.2]
Diffuse
Polymerised
Diffuse
Polymerised
Control
Sangunarine
ii
EcFtsZ
**
17.5 [95%CI 13.7, 21.4]
Control
Sanguinarine
iii
HpFtsZ
***
23 [95% CI 20.6, 25.4]
Control
Sanguinarine
E
i
***
22.4 [95% CI 15.8, 29.0]
Control
Berberine
ii
**
18.9 [95% CI, 16.1, 21.6]
Control
Berberine
iii
***
22.1 [95% CI 18.6, 25.6]
Control
Berberine

Figure 4

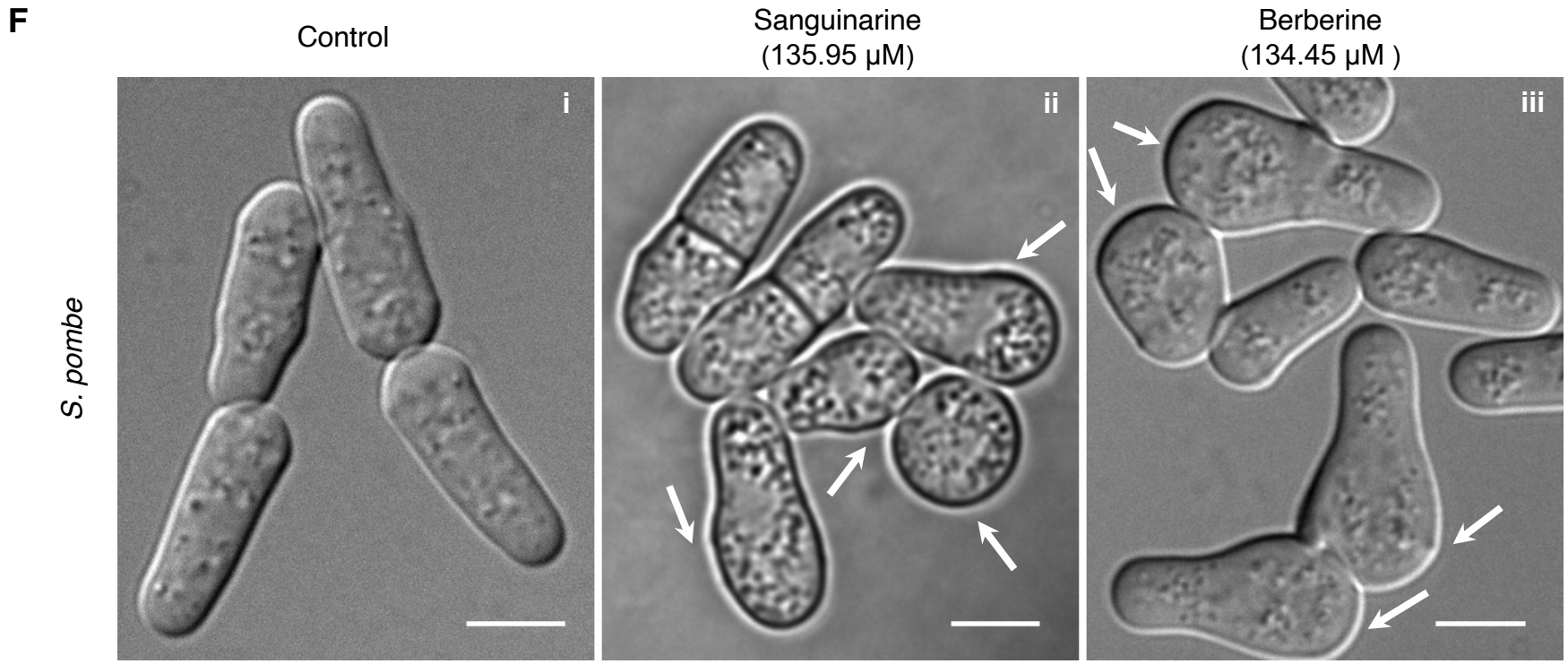
F
Control
Sanguinarine
(135.95 μM)
Berberine
(134.45 μM)
S. pombe
i
ii
iii

Figure 4. Inhibition of FtsZ polymerization of by sanguinarine and berberine. Fission yeast cultures expressing different bacterial FtsZ-GFP fusions were grown either in the absence or presence of the drug were mounted onto 1.6% agarose slides, and a epifluorescence microscope was used for the imaging. In control (untreated) cultures, an equivalent amount of DMSO was added. **(A – C)** Control (DMSO-treated) cells showed normal assembly of FtsZ polymers in fission yeast. **(A i)** SaFtsZ **(B i)** EcFtsZ and **(C i)** HpFtsZ. **(A ii – C ii)** Sanguinarine (20 μM) treated cells showed significant reduction in **(A ii)** SaFtsZ **(B ii)** EcFtsZ and **(C ii)** HpFtsZ. **(A iii – C iii)** Berberine (53.791 μM) inhibited the polymerisation of **(A iii)** SaFtsZ **(B iii)** EcFtsZ and **(C iii)** HpFtsZ. Scale bar represents 5 μm. **(D and E)** Quantification of the effects of **(D)** sanguinarine and **(E)** berberine on polymerisation of **(i – iii)** SaFtsZ, EcFtsZ and HpFtsZ, respectively. Light gray bars and dark gray bars represent cells having diffuse fluorescence and cells containing FtsZ polymers, respectively. The error bars shown are inferential and represent Mean ± 95% CI (N = 3). Asterix *** and ** indicate P-values ≤ 0.001 and ≤ 0.01 respectively. P-values were calculated the the two-sided proportions z-test. The mean difference between the proportion of cells carrying FtsZ polymers in the untreated and treated populations are also indicated as effect size [95% CI, lower bound, upper bound]. Biological replicates are independent liquid cultures starting from a fresh patch from frozen glycerol stocks. **(F)** Berberine and sanguinarine at high concentrations affect yeast cell morphology. *S. pombe* cultures were grown **(i)** in the absence of the drug or in the presence of **(ii)** sanguinarine (135.95 μM) or **(iii)** berberine (134.45 μM) and mounted onto 1.6% agarose slides and imaged. In control (untreated) cultures, an equivalent amount of DMSO was added. Fission yeast cells formed bulges at the poles as indicated by arrowheads. Scale bar represents 5 μm.

Figure 5

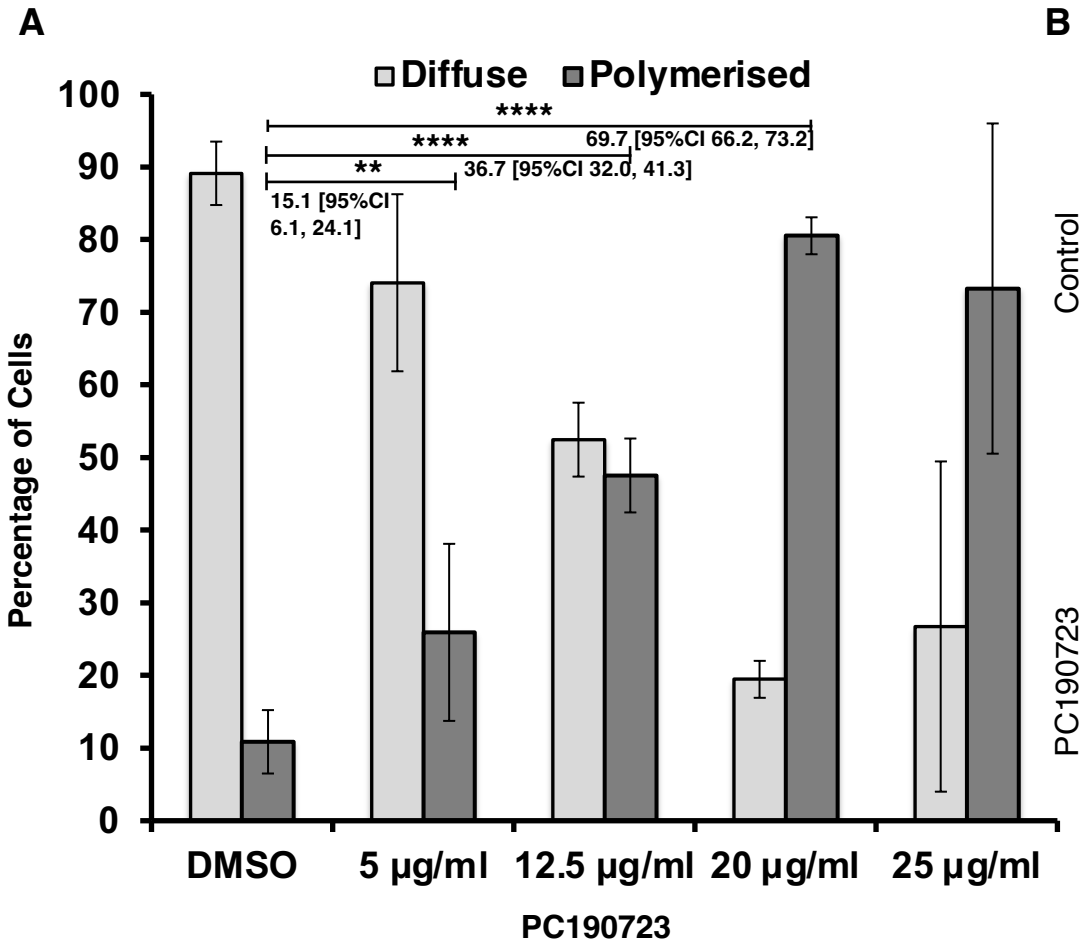
A
Diffuse
Polymerised
Percentage of Cells
100
90
80
70
60
50
40
30
20
10
0
****
****
69.7 [95%CI 66.2, 73.2]
**
36.7 [95%CI 32.0, 41.3]
15.1 [95%CI 6.1, 24.1]
DMSO
5 µg/ml
12.5 µg/ml
20 µg/ml
25 µg/ml
PC190723

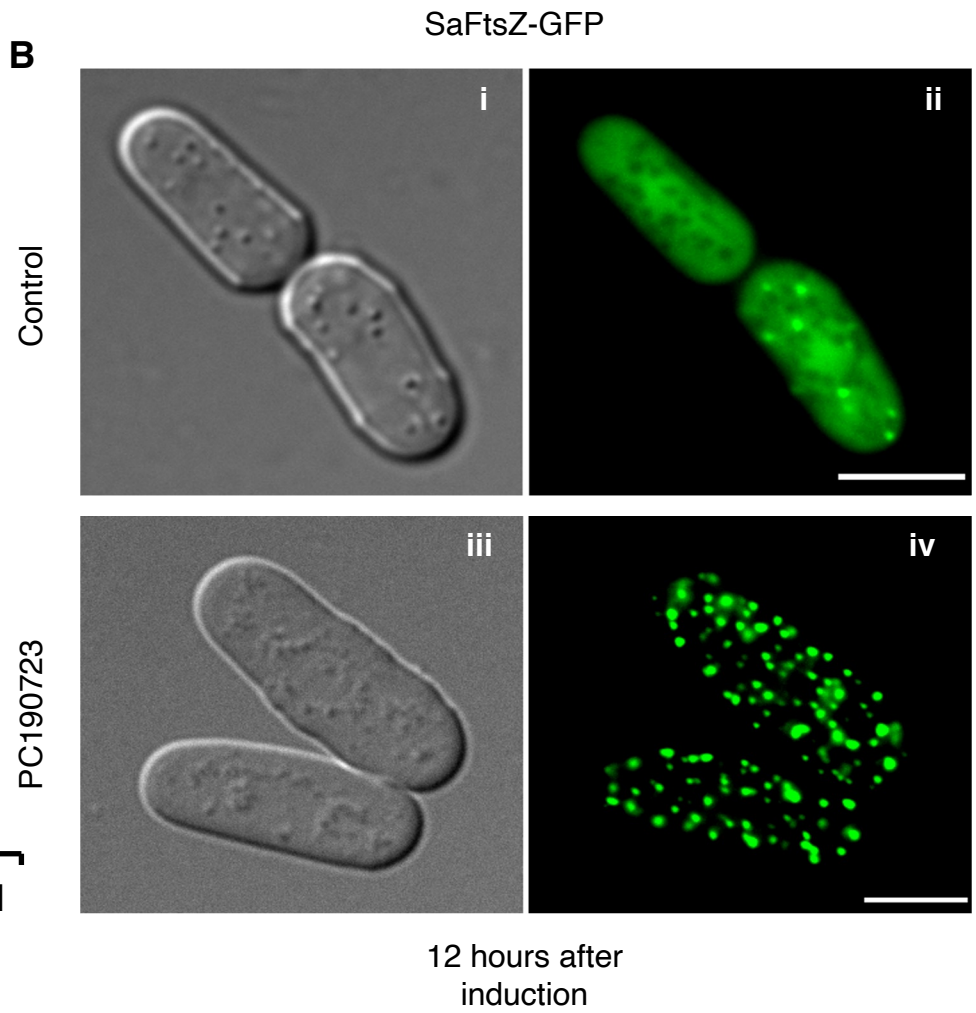
B
SaFtsZ-GFP
Control
PC190723
i
ii
iii
iv
12 hours after induction

Figure 5

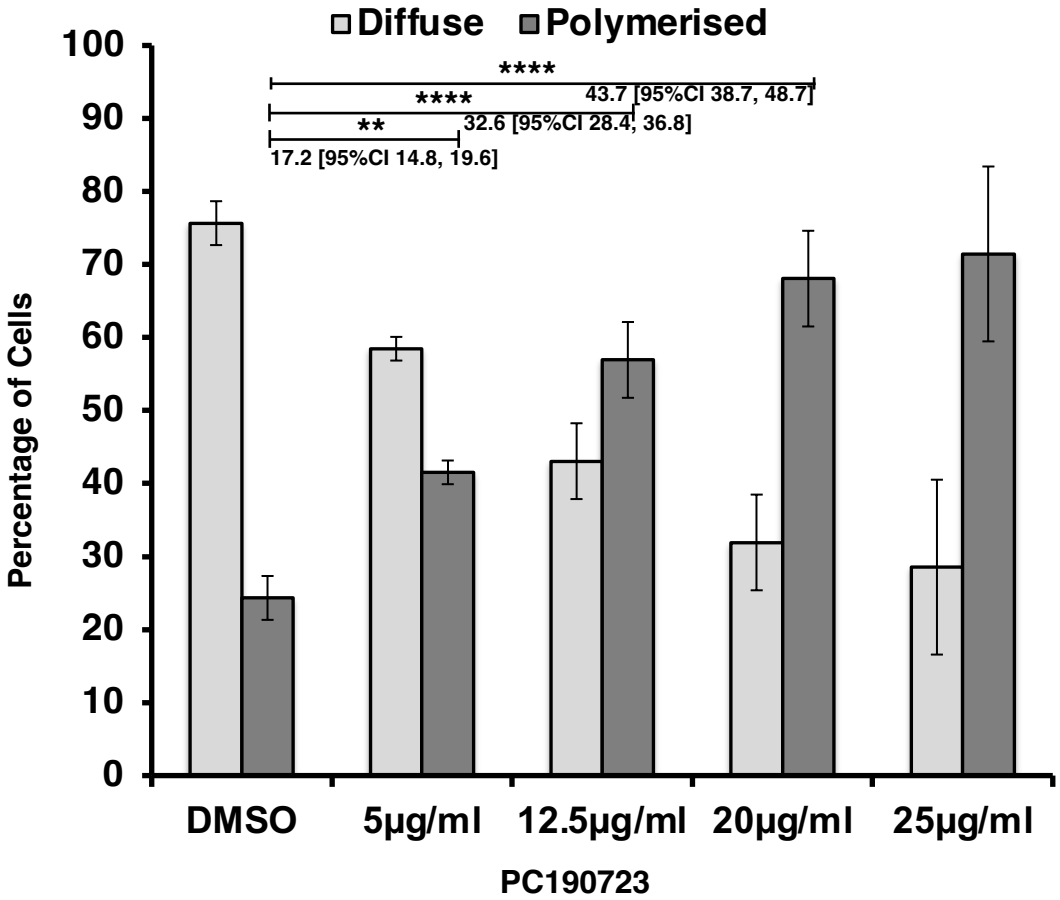
C
Diffuse
Polymerised
****
****
43.7 [95%CI 38.7, 48.7]
**
32.6 [95%CI 28.4, 36.8]
17.2 [95%CI 14.8, 19.6]
Percentage of Cells
100
90
80
70
60
50
40
30
20
10
0
DMSO
5µg/ml
12.5µg/ml
20µg/ml
25µg/ml
PC190723

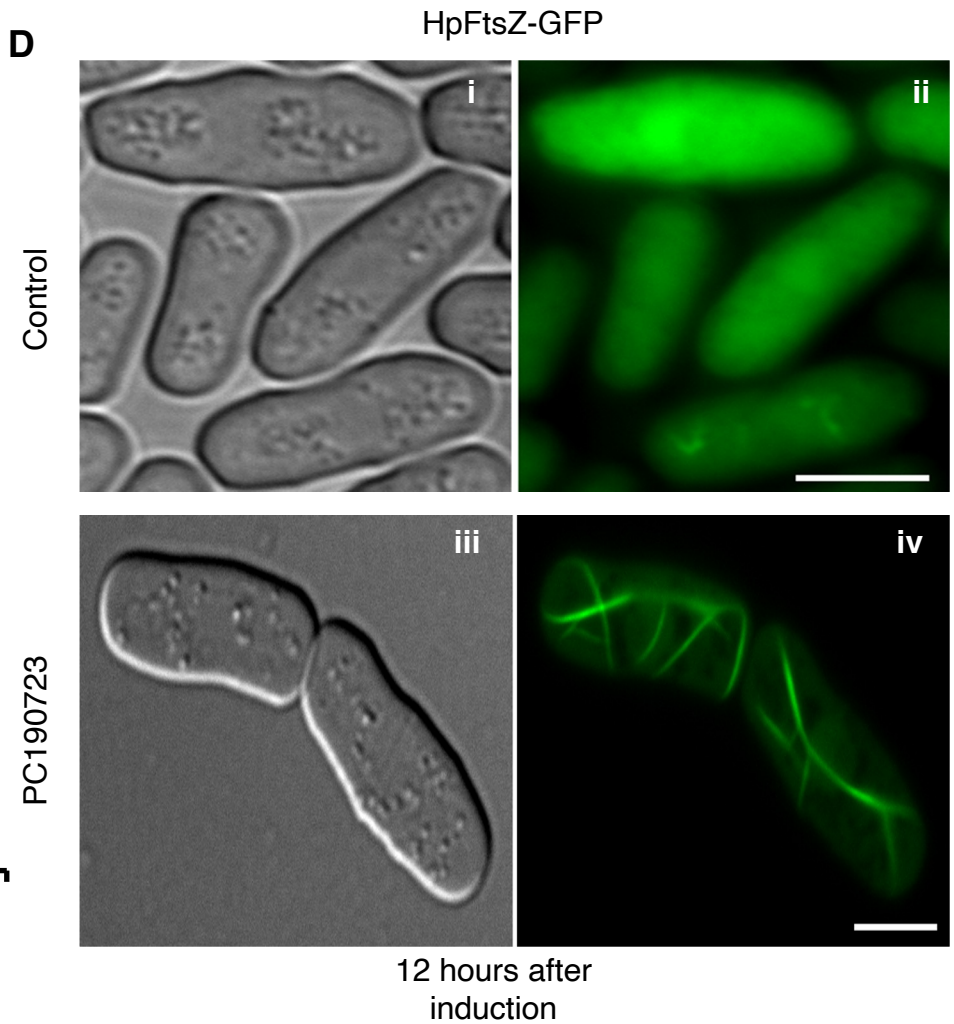
D
HpFtsZ-GFP
Control
PC190723
i
ii
iii
iv
12 hours after induction

Figure 5

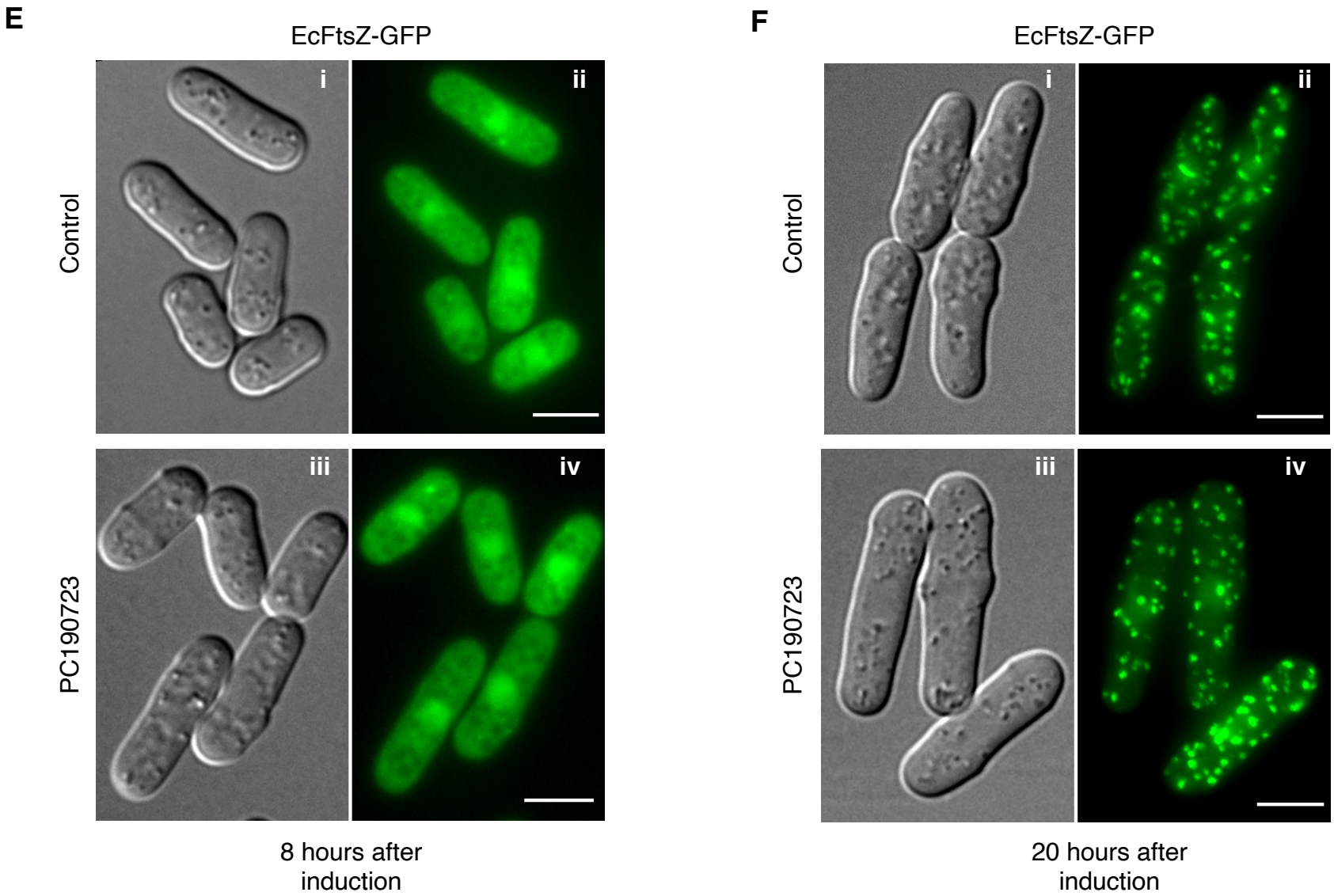
E
EcFtsZ-GFP
Control
PC190723
i
ii
iii
iv
8 hours after induction
F
EcFtsZ-GFP
Control
PC190723
i
ii
iii
iv
20 hours after induction

Figure 5. PC190723 induces polymerisation of SaFtsZ and HpFtsZ in fission yeast.

(A) Dose dependent effect of PC190723 on polymerisation of SaFtsZ. Graph showing percentage of cells having diffuse (light gray) and polymerised (dark gray) SaFtsZ in fission yeast in the absence (DMSO) or in the presence of PC190723 ranging from 5 – 25 µg / ml concentration. **(B)** Images showing the effect of PC190723 at 20 μg / ml on SaFtsZ. At a time-point when control (DMSO treated) cells expressing SaFtsZ-GFP show diffuse fluorescence (panel ii), cells grown with PC190723 (20 μg / ml) results in early appearance of SaFtsZ assemblies (panel iv). **(C)** Dose dependent effect of PC190723 on polymerisation of HpFtsZ. Graph showing percentage of cells having diffuse (light gray) and polymerised (dark gray) HpFtsZ in fission yeast in a range of PC190723 (5 – 25 µg / ml)concentrations. **(D)** Images showing the effect of PC190723 at 20 μg / ml on HpFtsZ. At a time-point when control (DMSO treated) cells expressing HpFtsZ-GFP show diffuse fluorescence (panel ii), cells grown with PC190723 (20 μg / ml) results in early appearance of HpFtsZ polymers (panel iv). *S. pombe* cells expressing SaFtsZ or HpFtsZ were grown at 30ºC in the absence of thiamine for 8 – 10 hours before DMSO or PC190723 was added to the cultures. The cultures were further incubated 4 hours at 30ºC before imaging or counting. **(E) and (F)** Images showing the effect of PC190723 at 20 μg / ml on EcFtsZ. **(E)** Unlike, Sa or HpFtsZ, cells expressing EcFtsZ-GFP and grown in the presence of PC190723 (20 μg / ml), exhibit diffuse fluorescence similar to that of control (DMSO treated) cells at early time-points. *S. pombe* cells expressing EcFtsZ were grown at 30ºC in the absence of thiamine for 4 – 6 hours before DMSO or PC190723 was added to the cultures. The cultures were further incubated 4 hours at 30ºC before imaging or counting. **(F)** At longer induction times (20 hours) both control (DMSO) and PC190723 treated cells formed EcFtsZ structures. DMSO or PC190723 was added to the cultures after 6 - 8 hours of growth in the absence of thiamine and incubated further at 30ºC. The error bars shown in **A** and **C** are inferential and represent the 95% CI (N = 3). ****, *** and ** indicate

P-values ≤ 0.0001, ≤ 0.001 and ≤ 0.01 respectively. P-values were calculated using the the two-sided proportions z-test. The mean difference between the proportion of cells carrying FtsZ polymers in the untreated and treated populations are also indicated as effect size [95% CI, lower bound, upper bound]. Scale bar represents 5 μm.

Figure 6

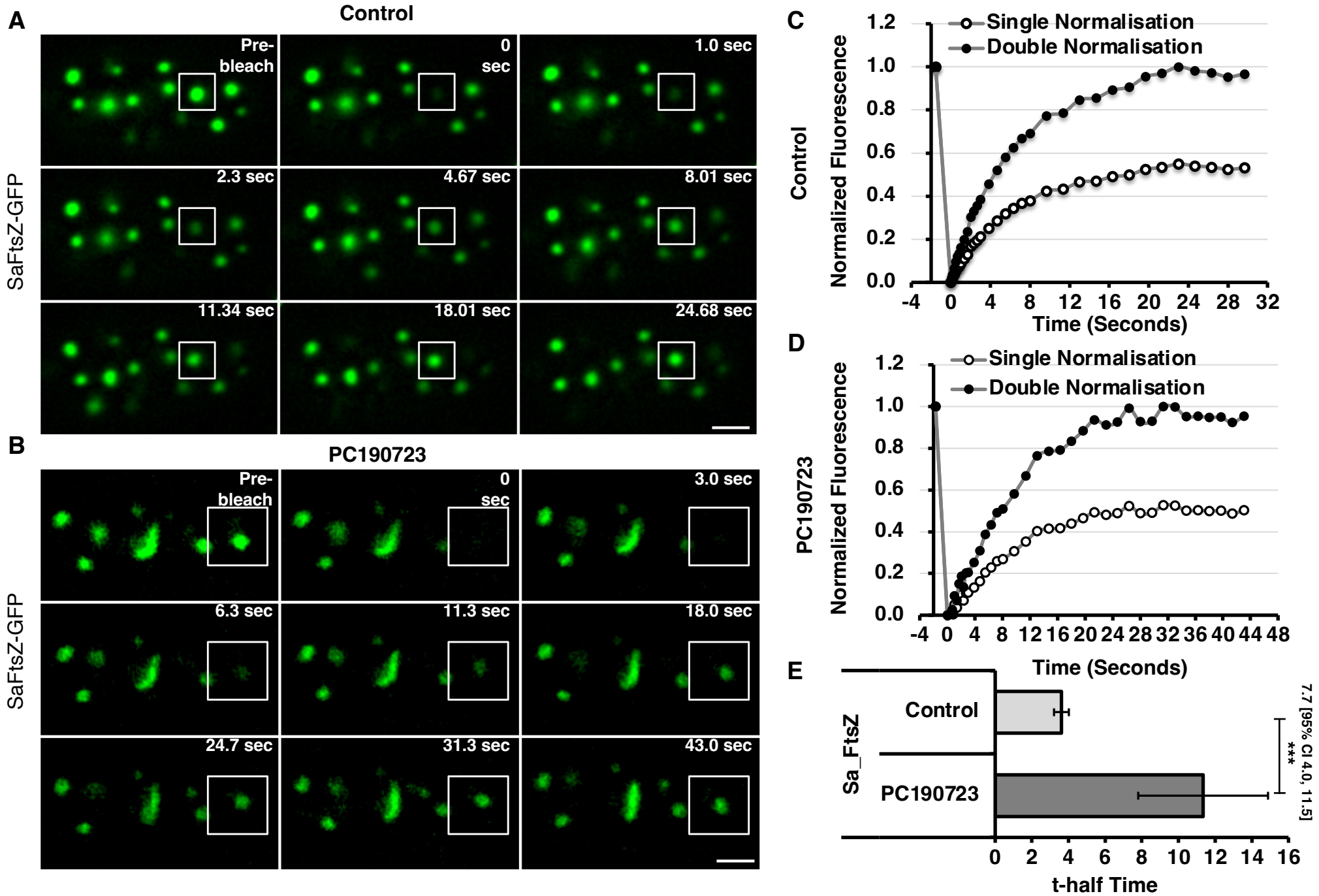
A
Control
SaFtsZ-GFP
Pre-bleach
0 sec
1.0 sec
2.3 sec
4.67 sec
8.01 sec
11.34 sec
18.01 sec
24.68 sec
B
PC190723
SaFtsZ-GFP
Pre-bleach
0 sec
3.0 sec
6.3 sec
11.3 sec
18.0 sec
24.7 sec
31.3 sec
43.0 sec
C
Control
Single Normalisation
Double Normalisation
Normalized Fluorescence
Time (Seconds)
D
PC190723
Single Normalisation
Double Normalisation
Normalized Fluorescence
Time (Seconds)
E
Sa_FtsZ
Control
PC190723
***
7.7 [95% CI 4.0, 11.5]
t-half Time

Figure 6

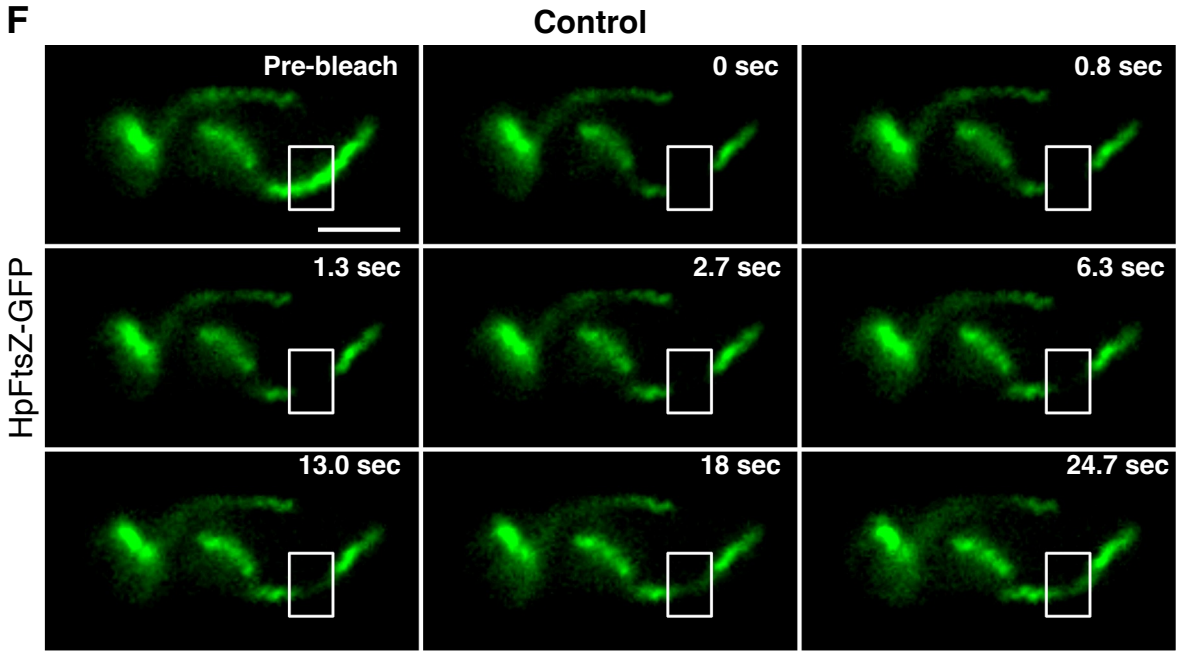
F
Control
HpFtsZ-GFP
Pre-bleach
0 sec
0.8 sec
1.3 sec
2.7 sec
6.3 sec
13.0 sec
18 sec
24.7 sec

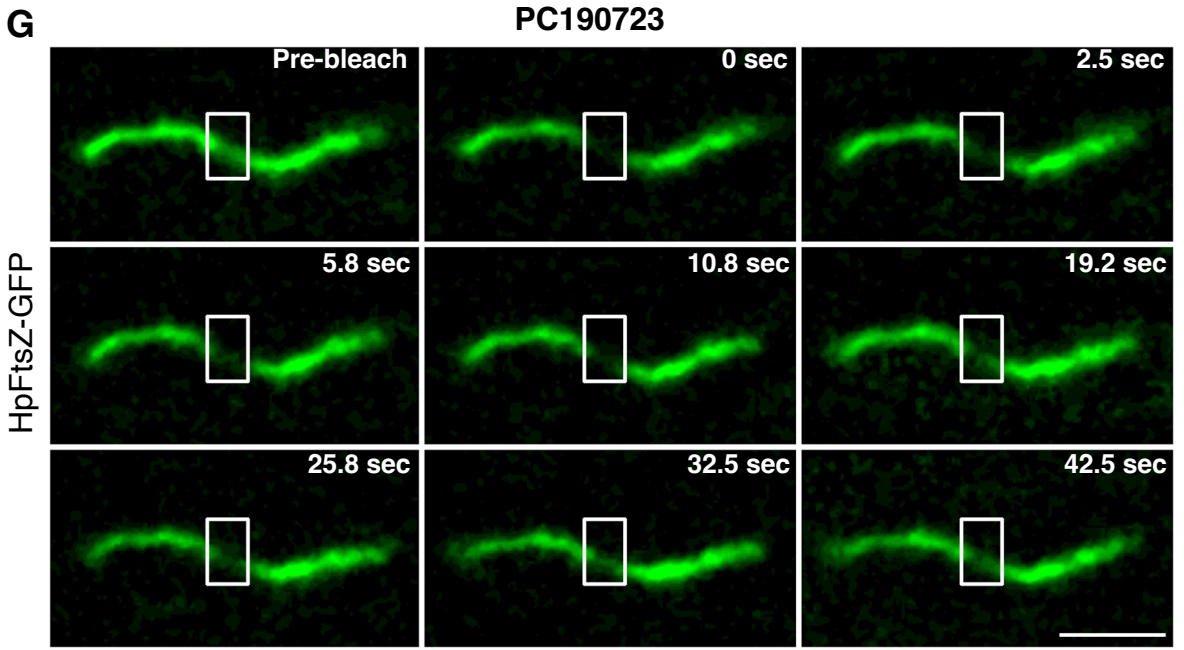
G
PC190723
HpFtsZ-GFP
Pre-bleach
0 sec
2.5 sec
5.8 sec
10.8 sec
19.2 sec
25.8 sec
32.5 sec
42.5 sec

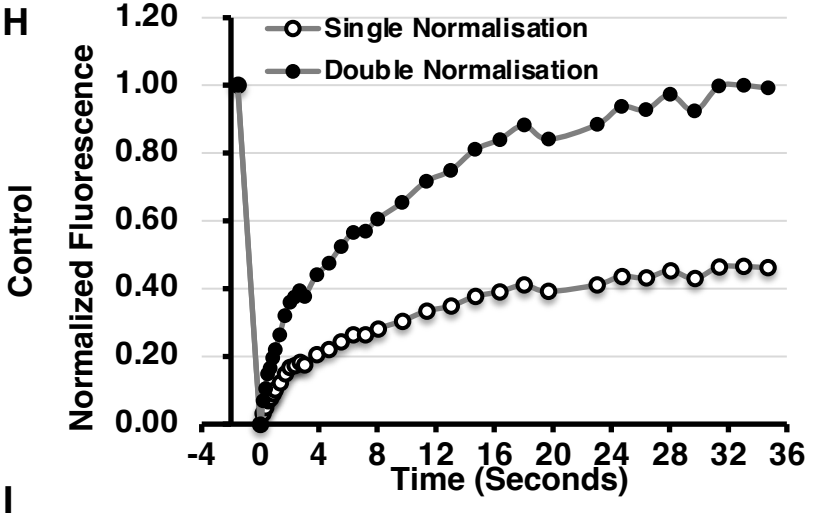
H
Control
Single Normalisation
Double Normalisation
Normalized Fluorescence
1.20
1.00
0.80
0.60
0.40
0.20
0.00
-4 0 4 8 12 16 20 24 28 32 36
Time (Seconds)

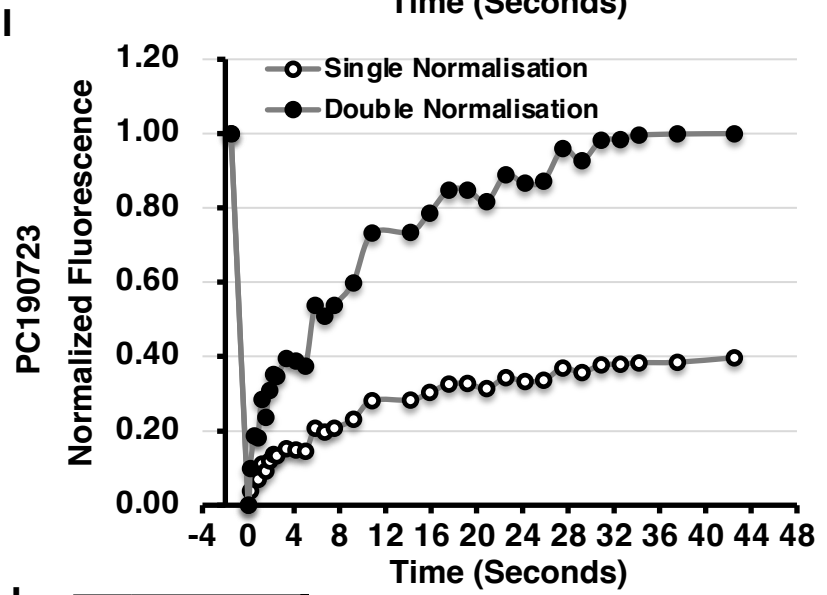
I
PC190723
Single Normalisation
Double Normalisation
Normalized Fluorescence
1.20
1.00
0.80
0.60
0.40
0.20
0.00
-4 0 4 8 12 16 20 24 28 32 36 40 44 48
Time (Seconds)

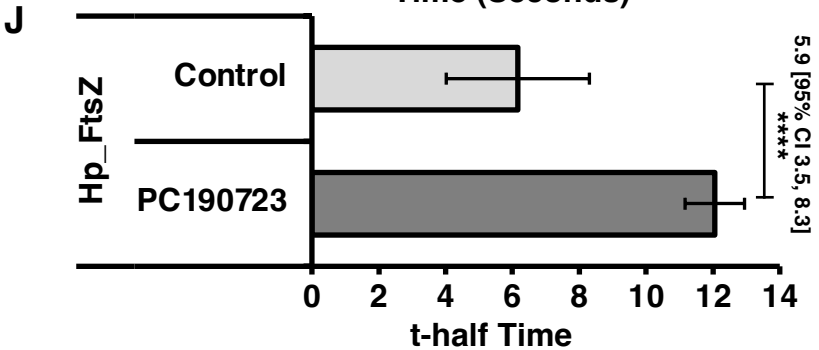
J
Hp_FtsZ
Control
PC190723
5.9 [95% CI 3.5, 8.3]
****
0 2 4 6 8 10 12 14
t-half Time

Figure 6. PC190723 reduces the polymer turnover rates of SaFtsZ and HpFtsZ.

Fluorescence recovery after photobleaching (FRAP) of **(A)** control (DMSO treated) and **(B)** PC190723 (20 µg/ml) treated cells expressing SaFtsZ. Fission yeast cultures expressing SaFtsZ-GFP were mounted onto agarose slides, and imaged with epifluorescence microscope. Fluorescence bleaching at selected ROIs were carried out using 488 nm laser line. Fluorescence intensities during recovery was quantified and a representative graph plotting the normalised intensities is shown in **(C)** for control (DMSO treated) cells and **(D)** PC190723 treated cells. **(E)** Quantification of the half-time ($t_{1/2}$) values for control (N = 10) and PC190723 treated (N = 10) cells. Fluorescence recovery after photobleaching (FRAP) of **(F)** control (DMSO treated) and **(G)** PC190723 (20 µg/ml) treated cells expressing HpFtsZ. Fission yeast cultures expressing HpFtsZ-GFP were imaged as mentioned above. Normalised fluorescence intensities of a representative experiment is plotted for **(H)** control (DMSO treated) cells and **(I)** PC190723 treated cells. **(J)** Quantification of the half-time ($t_{1/2}$) values for control (N = 10) and PC190723 treated (N = 10) cells. The $t_{1/2}$ values mentioned in the text were obtained by fitting the fluorescence recovery curves to a single exponential curve $F(t)= C(1 - e^{-kt})$ using Excel's Solver function and calculated from $t_{1/2} = \ln(2)/k$.

An unpaired two-tailed Student's t-test was used to assess the statistical significance. P-values ≤ 0.0001 and ≤ 0.001 are indicated by **** and *** respectively. The mean difference between the proportion of cells carrying FtsZ polymers in the untreated and treated populations are also indicated as effect size [95% CI, lower bound, upper bound]. Scale bar represents 5 µm.

Figure 7

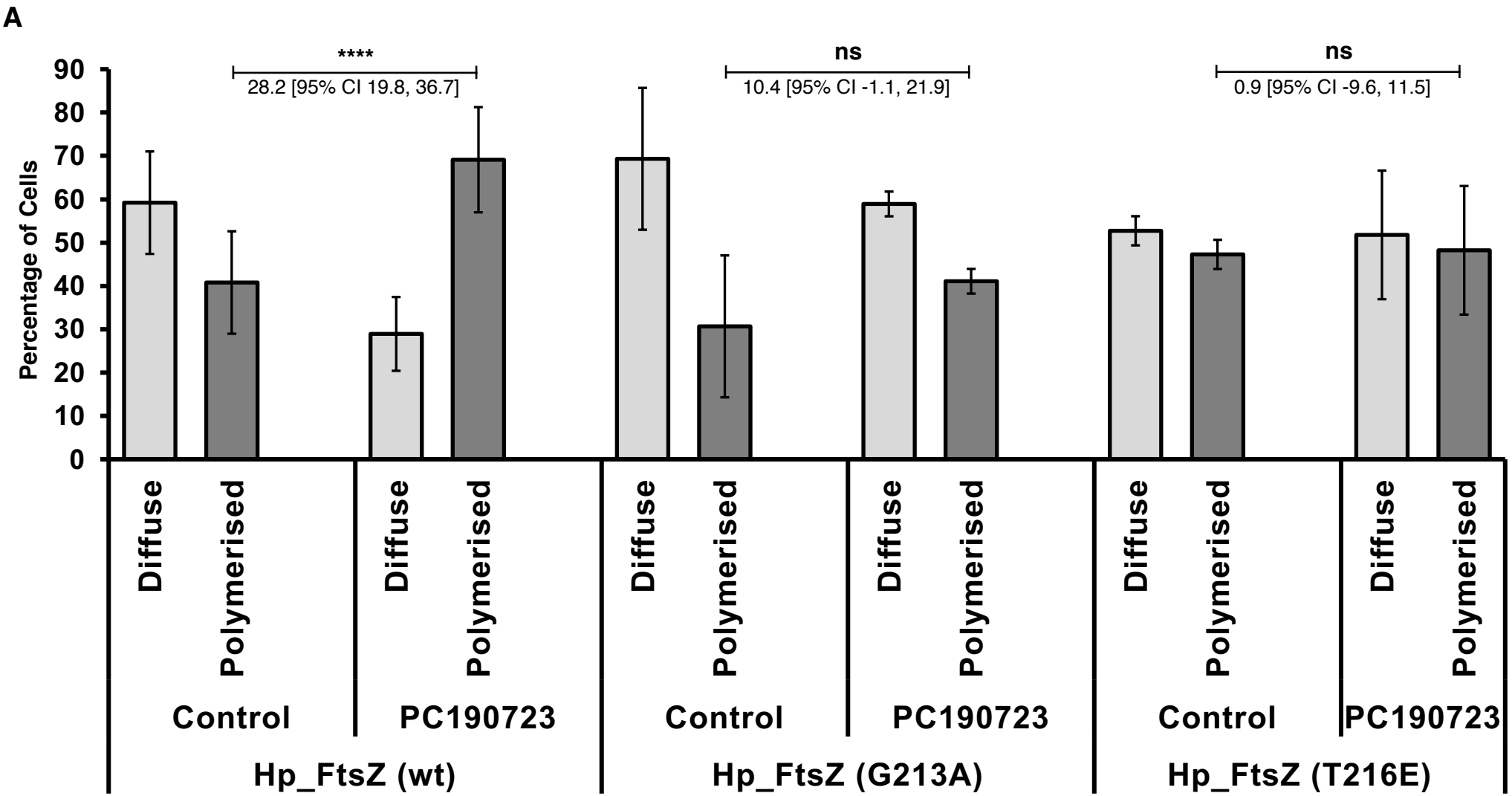
A
****
28.2 [95% CI 19.8, 36.7]
ns
10.4 [95% CI -1.1, 21.9]
ns
0.9 [95% CI -9.6, 11.5]
Percentage of Cells
90
80
70
60
50
40
30
20
10
0
Diffuse
Polymerised
Control
PC190723
Hp_FtsZ (wt)
Hp_FtsZ (G213A)
Hp_FtsZ (T216E)

Figure 7

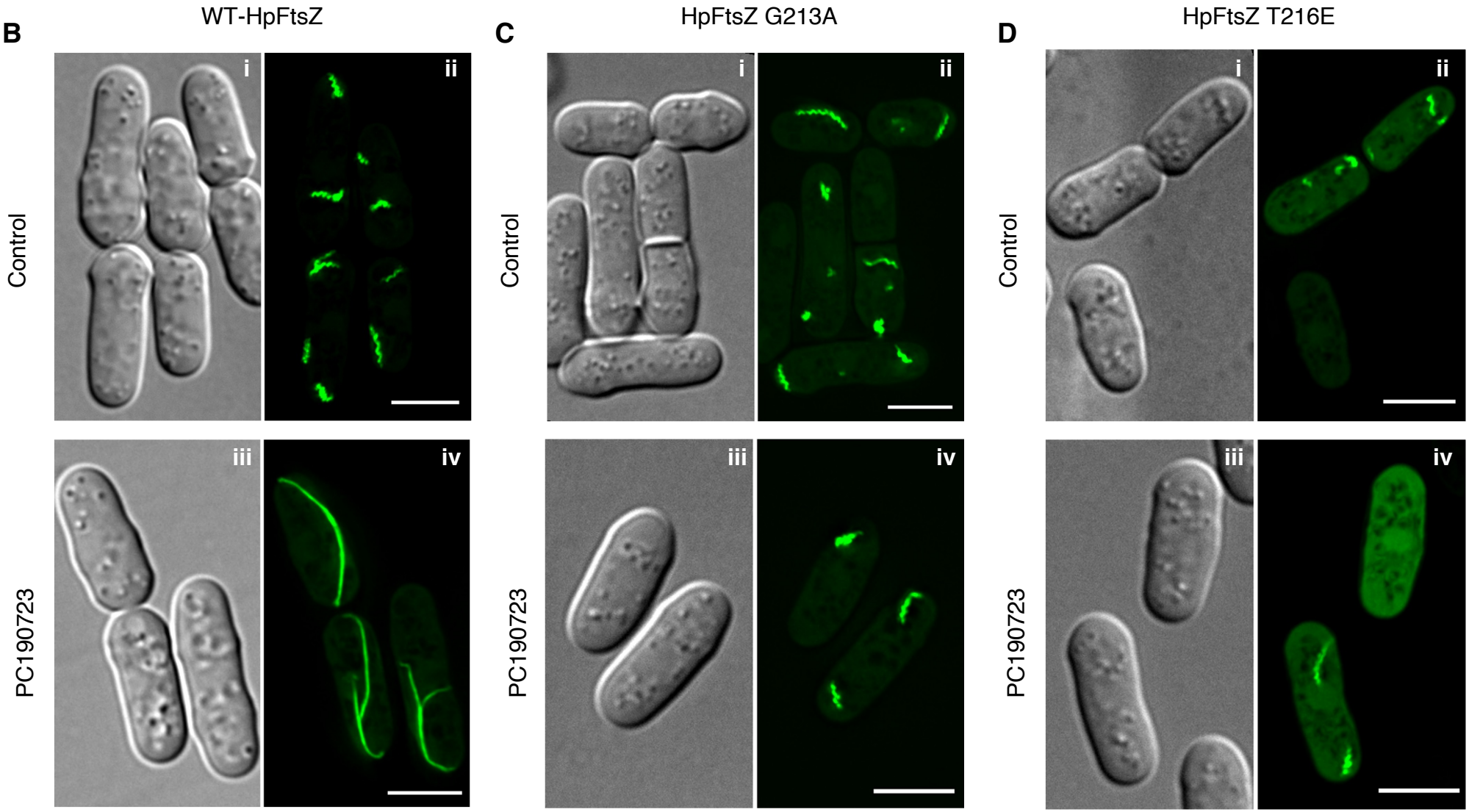
B
WT-HpFtsZ
C
HpFtsZ G213A
D
HpFtsZ T216E
Control
PC190723
i
ii
iii
iv

Figure 7. Determinants of resistance to PC190723 in HpFtsZ. *S. pombe* cultures carrying HpFtsZ^{WT}, HpFtsZ^{G213A} or HpFtsZ^{T216E} were grown for 8 – 10 hours in the absence of PC190723 and then sub-cultured in presence of drug at 30°C for 4 hours to allow the sufficient expression of the proteins and imaged using an epifluorescence microscope. While G213A is predicted to act as a steric block to PC190723, T216E would result in salt-bridge interactions with R326 (R307 in EcFtsZ^{WT}). **(A)** Effect of PC190723 on polymerisation of HpFtsZ mutants G213A and T216E. Graph shows percentage of cells having diffuse (light gray) and polymerised (dark gray) HpFtsZ in fission yeast in the absence (control) or presence of PC190723 (20 µg / ml). Images showing the effect of PC190723 at 20 μg / ml on **(B)** HpFtsZ^{WT} (panel iv), **(C)** HpFtsZ^{G213A} (panel iv) and **(D)** HpFtsZ^{T216E} (panel iv). At a time-point when control (DMSO treated) cells expressing HpFtsZ^{WT} show short polymers (panel ii), cells grown with PC190723 (20 μg / ml) shows stabilisation of longer HpFtsZ polymers (panel iv). However, cells expressing **(C)** HpFtsZ^{G213A} (panel iv) and **(D)** HpFtsZ^{T216E} (panel iv) exhibit short polymers or diffuse fluorescence in the presence of 20 μg / ml of PC190723 like in DMSO treated cells expressing **(C)** HpFtsZ^{G213A} (panel ii) and **(D)** HpFtsZ^{T216E} (panel ii).
The error bars shown are inferential and represent the 95% CI (N = 3). **** and ns indicate P-values ≤ 0.0001 and > 0.05 respectively. P-values were calculated from the two-sided proportions z-test. The mean difference between the proportion of cells carrying FtsZ polymers in the untreated and treated populations are also indicated as effect size [95% CI, lower bound, upper bound]. Scale bar represents 5 µm.

Figure 8

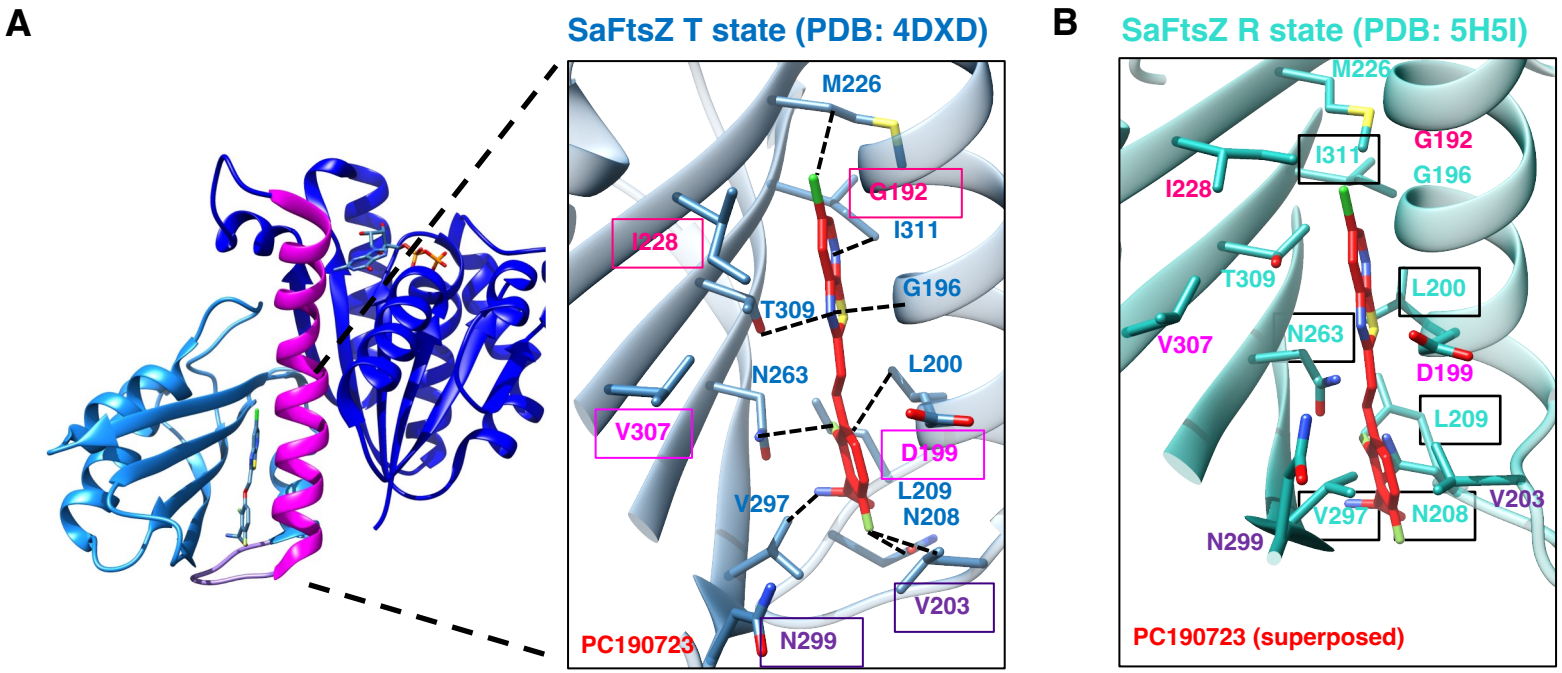

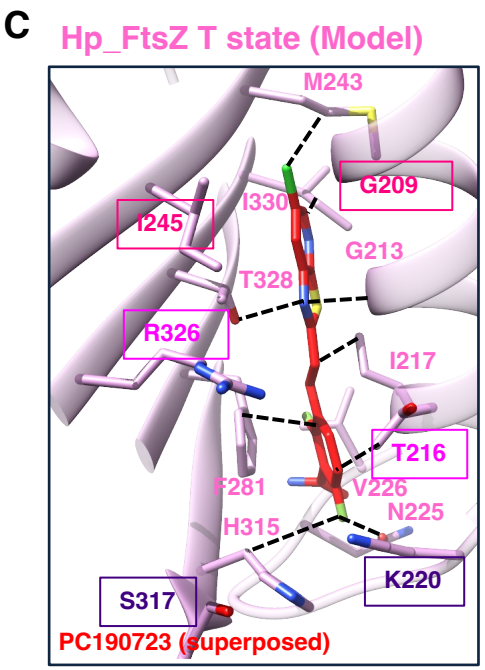

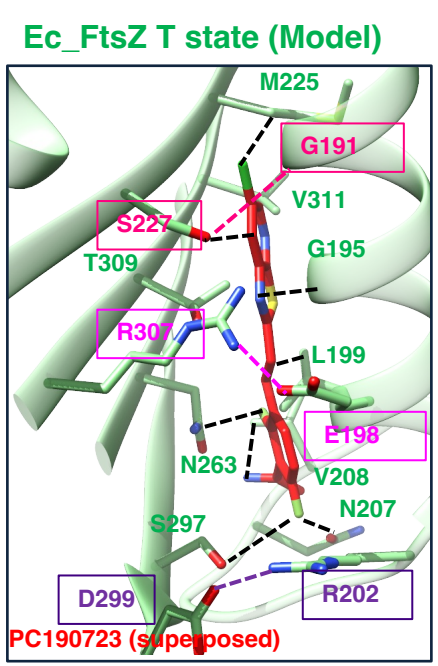

E

Interaction 1 (Hydrogen bond)

H.pylori	G I G	246	No	
E.coli	G S G	228	Yes	
S.aureus	G I G	229	No	
B.subtilis	G I G	229	No	

Interaction 2 (Salt Bridge)

H.pylori	S T I	217	V R V	327	No
E.coli	A E L	199	L R V	308	Yes
S.aureus	S D L	200	I V V	308	No
B.subtilis	S D L	200	I V V	308	No

Interaction 3 (Salt bridge)

H.pylori	T K P	221	T S D	318	No
E.coli	T R P	203	L D P	300	Yes
S.aureus	A V S	204	I N P	300	No
B.subtilis	A T P	204	I N E	300	No

Figure 8. PC190723 can bind to the T state conformation of HpFtsZ. (A) Overall structure of SaFtsZ bound to PC190723 (PDB ID: 4DXD; NBD - dark blue, H7 helix- magenta, T7 loop- purple and CTD- blue) with a zoomed-in structure of PC190723 binding cleft (PDB ID: 4DXD; T state, open cleft) as inset. Residues of FtsZ which interact with PC190723 (PDB ID- 4DXD) are shown in stick representation. **(B)** PC190723 binding cleft in R state conformation (PDB ID: 5H5I; sea green) is closed and the residues clash with the drug (highlighted in black boxes) and prevent the binding of the drug. **(C)** HpFtsZ modelled in T state structure (light pink) and superimposed on PDB 4DXD. There are no clashes with the drug and F281 could stack against the benzamide ring of PC190723. HpFtsZ does not possess any interaction that could potentially block the cleft. **(D)** PC190723 placed (by superposition of PDB 4DXD onto EcFtsZ T state model) in the pocket in EcFtsZ modelled in T state structure (green) highlight that there are two salt bridges, R309 and E198; D299 and R202 (shown in magenta and purple respectively) and a hydrogen bond between OH group of S226 and main chain of G191 in H7 helix (shown in dark pink) which could block the cleft. **(E)** Residues in HpFtsZ and SaFtsZ corresponding to residues of EcFtsZ which might block the PC binding cleft due to three interaction types highlighted in the figure panels.

In all panels, residues which are labelled in dark pink, magenta and purple fonts and boxed are the corresponding residues which form salt bridge and hydrogen bonds in EcFtsZ. Dotted lines represent interactions at distances ≤ 4Å.

Supplementary Figures

Figure S1

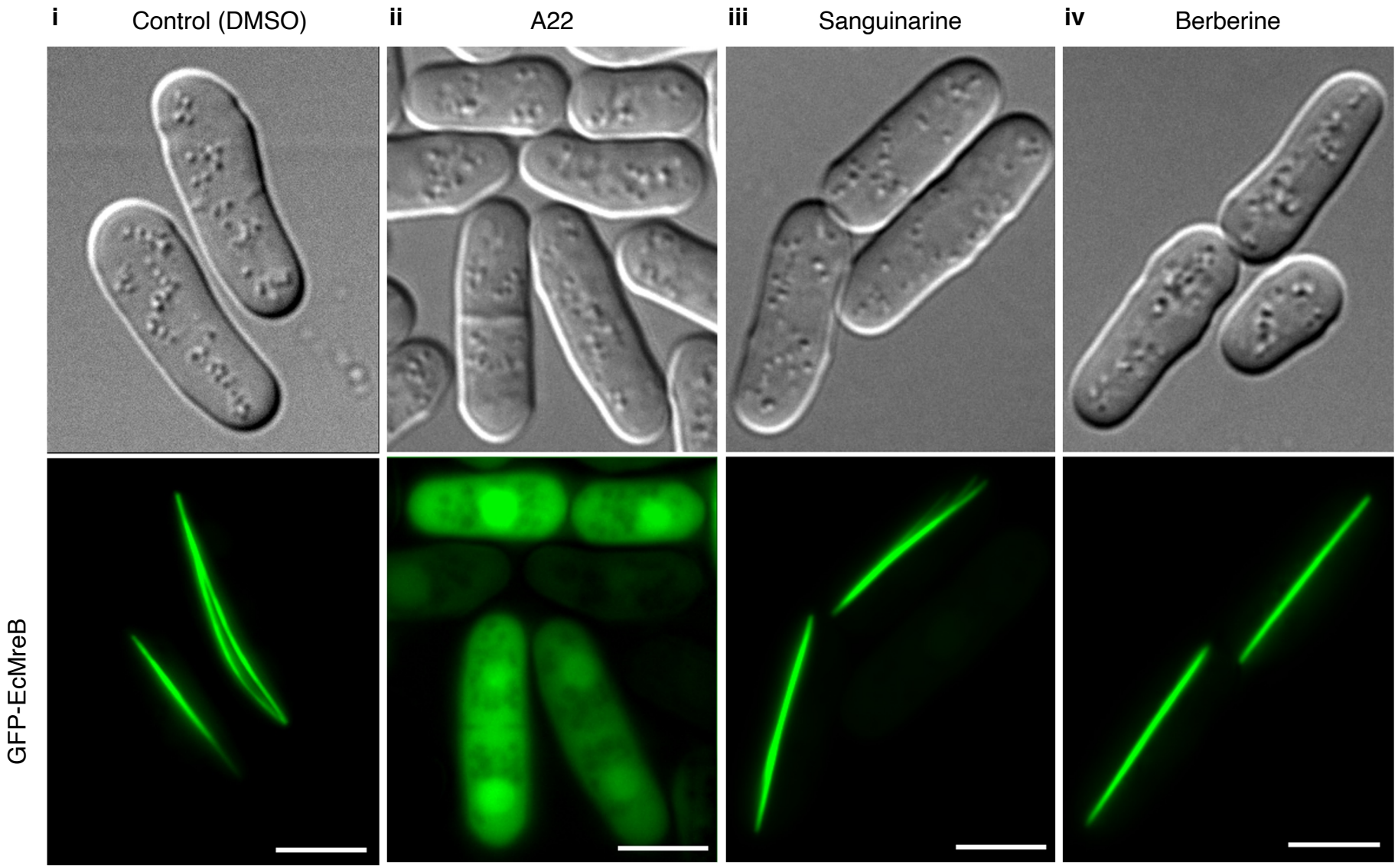
i
Control (DMSO)
ii
A22
iii
Sanguinarine
iv
Berberine
GFP-EcMreB

Supplementary Figure Legends:

Figure S1. Sanguinarine and berberine do not affect the polymerization of the *E. coli* actin homolog MreB. (i) DMSO-treated cells showed linear array of EcMreB polymers in fission yeast. **(ii)** MreB inhibitor A22 (73.64 μM) prevented polymerisation of EcMreB. **(iii)** sanguinarine (20 μM) and **(iv)** berberine (53.791 μM) treated cells showed MreB bundles similar to control cells suggesting failure to inhibit MreB assembly. Scale bar represents 5 μm.

Figure S2

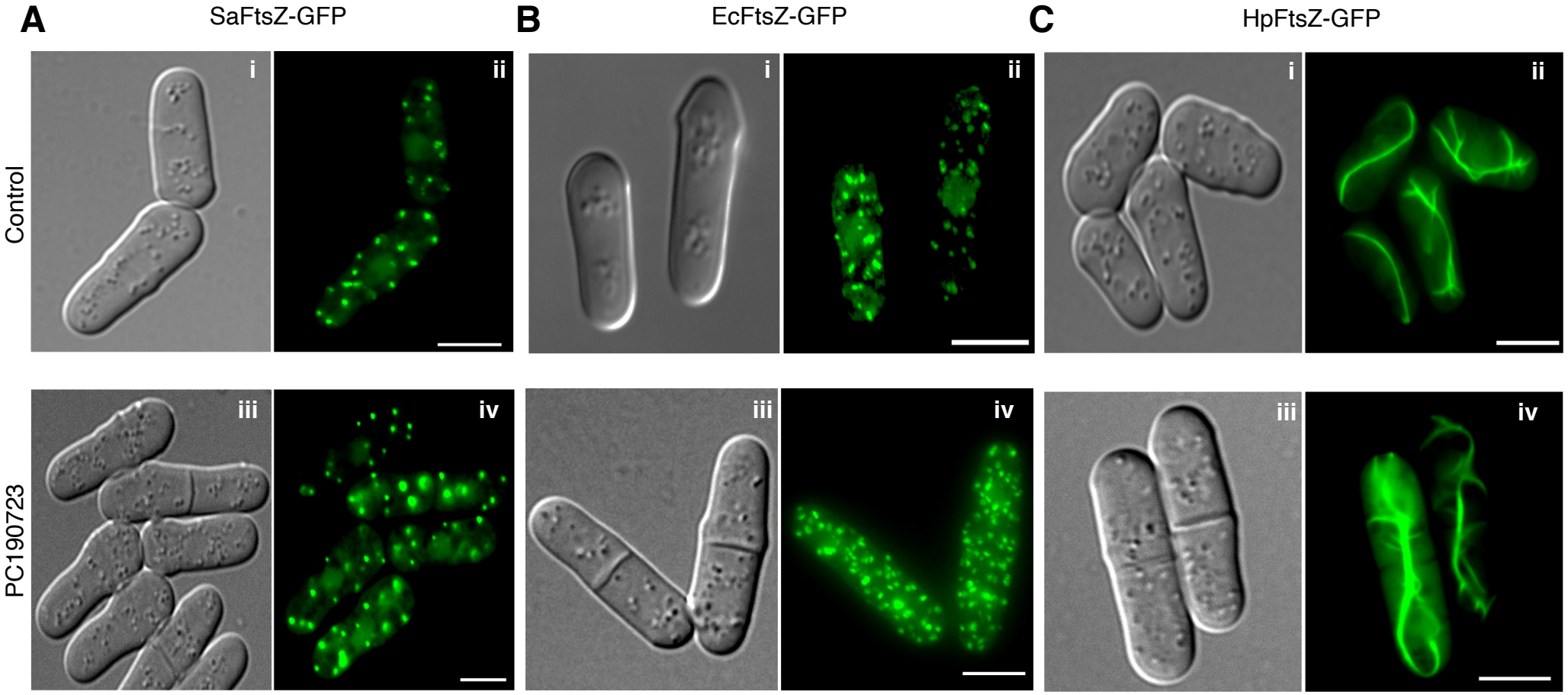
A
SaFtsZ-GFP
B
EcFtsZ-GFP
C
HpFtsZ-GFP
Control
PC190723
i
ii
iii
iv

Figure S2. PC190723 does not affect the FtsZ structures in fission yeast after assembly of FtsZ. Fission yeast cultures expressing different bacterial FtsZ-GFP fusions **(A)** EcFtsZ_GFP, **(B)** SaFtsZ_GFP and **(C)** HpFtsZ_GFP were mounted onto 1.6% agarose slides before imaging using an epifluorescence microscope. Addition of PC190723 (20 µg/ml) after the appearance of FtsZ polymers shows no significant effect on FtsZ polymers **(A – C, panels iv)**. In control (untreated) cultures **(A – C, panels ii)**, an equivalent amount of DMSO was added. *S. pombe* cells expressing EcFtsZ, SaFtsZ or HpFtsZ were grown at 30ºC in the absence of thiamine for 20 – 24 hours before DMSO or PC190723 was added to the cultures. The cultures were further incubated 4 hours at 30ºC and imaged. Scale bar represents 5 µm.

Figure S3

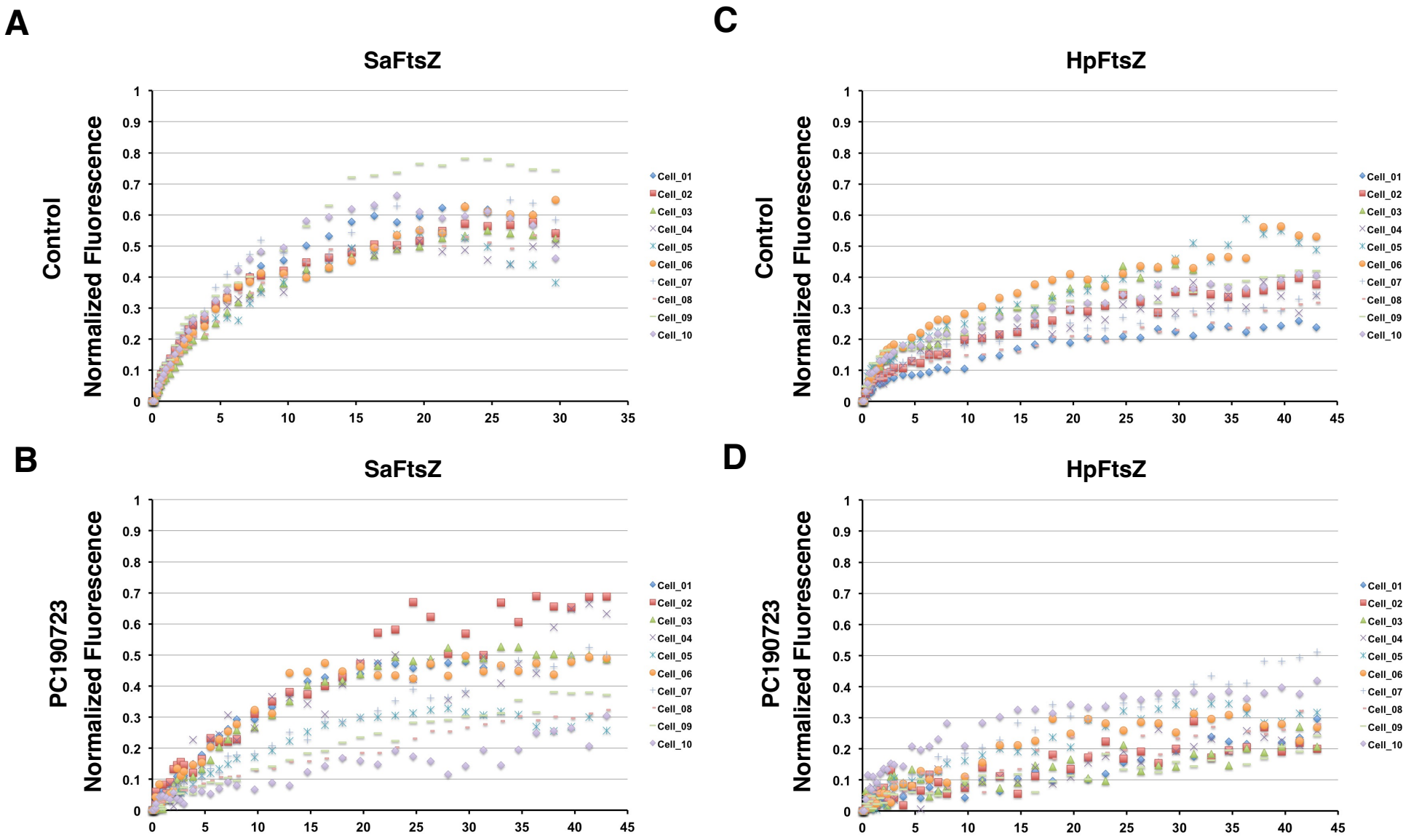
A
SaFtsZ
Control
Normalized Fluorescence
B
SaFtsZ
PC190723
Normalized Fluorescence
C
HpFtsZ
Control
Normalized Fluorescence
D
HpFtsZ
PC190723
Normalized Fluorescence
Cell_01
Cell_02
Cell_03
Cell_04
Cell_05
Cell_06
Cell_07
Cell_08
Cell_09
Cell_10

Figure S3. PC190723 reduces the polymer turnover rates of SaFtsZ and HpFtsZ. Graphs showing the fluorescence recovery after photobleaching (FRAP) of **(A & B)** SaFtsZ-GFP or **(C & D)** HpFtsZ-GFP assemblies in fission yeast. **(A & C)** Control (DMSO treated) cells and **(B & D)** PC190723 (20 µg / ml) treated cells. Fluorescence intensities during recovery was quantified and single normalised intensities were plotted against time.

Figure S4

A

```
                   *  *     *     *   *                          *
H.pylori           V R A V S G I S T I I T K P G N I N V D F A D L K S A L G F K G F A L M G I G 245
M.jannaschii       I N A V K G L V E L I T K D G L I N V D F A D V K A V M N N G G L A M I G I G 253
E.coli             K G A V Q G I A E L I T R P G L M N V D F A D V R T V M S E M G Y A M M G S G 227
P.aeruginosa       A G A V R G I S D I I K R P G M I N V D F A D V K T V M S E M G M A M M G T G 228
T.maritima         H Q G V K G I S E L I T K R G Y I N L D F A D I E S V M K D A G A A I L G I G 238
M.tuberculosis     L N G V Q G I T D L I T T P G L I N V D F A D V K G I M S G A G T A L M G I G 225
T.fusca            L S G V Q G I T D L I T T P G L I N L D F A D V K S V M S G A G S A L M G I G 238
S.aureus           R Q G V Q G I S D L I A V S G E V N L D F A D V K T I M S N Q G S A L M G I G 228
B.subtilis         R Q G V Q G I S D L I A T P G L I N L D F A D V K T I M S N K G S A L M G I G 228

                     *                     *   *
H.pylori           G Q H T S D N I P I D H V R V T I I A 332
M.jannaschii       G A T I D E N L - E N T V R V L L V I 337
E.coli             G T S L D P D M - N D E L R V T V V A 312
P.aeruginosa       G T V I D A D M - R D E L H V T V V A 313
T.maritima         G L I F D D E V P D D E I R V I F I A 323
M.tuberculosis     G T V I D D S L - G D E V R V T V I A 310
T.fusca            G A V I D D A L - G D E V R V T V I A 323
S.aureus           G T V I N P E L - Q D E I V V T V I A 312
B.subtilis         G S V I N E N L - K D E I V V T V I A 312

                     *
H.pylori           V F F E H 284
M.jannaschii       I H V M G 291
E.coli             V N I T A 266
P.aeruginosa       V N I T A 267
T.maritima         F N I T A 276
M.tuberculosis     M S I A G 273
T.fusca            L S I Q G 276
S.aureus           M N I T G 266
B.subtilis         M N I T G 266
```

B

Residues interacting with PC190723 (SaFtsZ)	Corresponding residues in *Hp*FtsZ
G196	G213
L200	I217
V203	K220 (does not interact)
N208	N225
L209	V226
M226	M243
N263	F281 (stacking)
V297	H315 (does not interact)
T309	T328
I311	I330

Figure S4. (A) Multiple sequence alignment of FtsZs from different bacteria; stars (*) represent the residues in SaFtsZ which interacts with PC190723. **(B)** Residues interacting with PC190723 in SaFtsZ, and their corresponding residues in HpFtsZ.

Figure S5

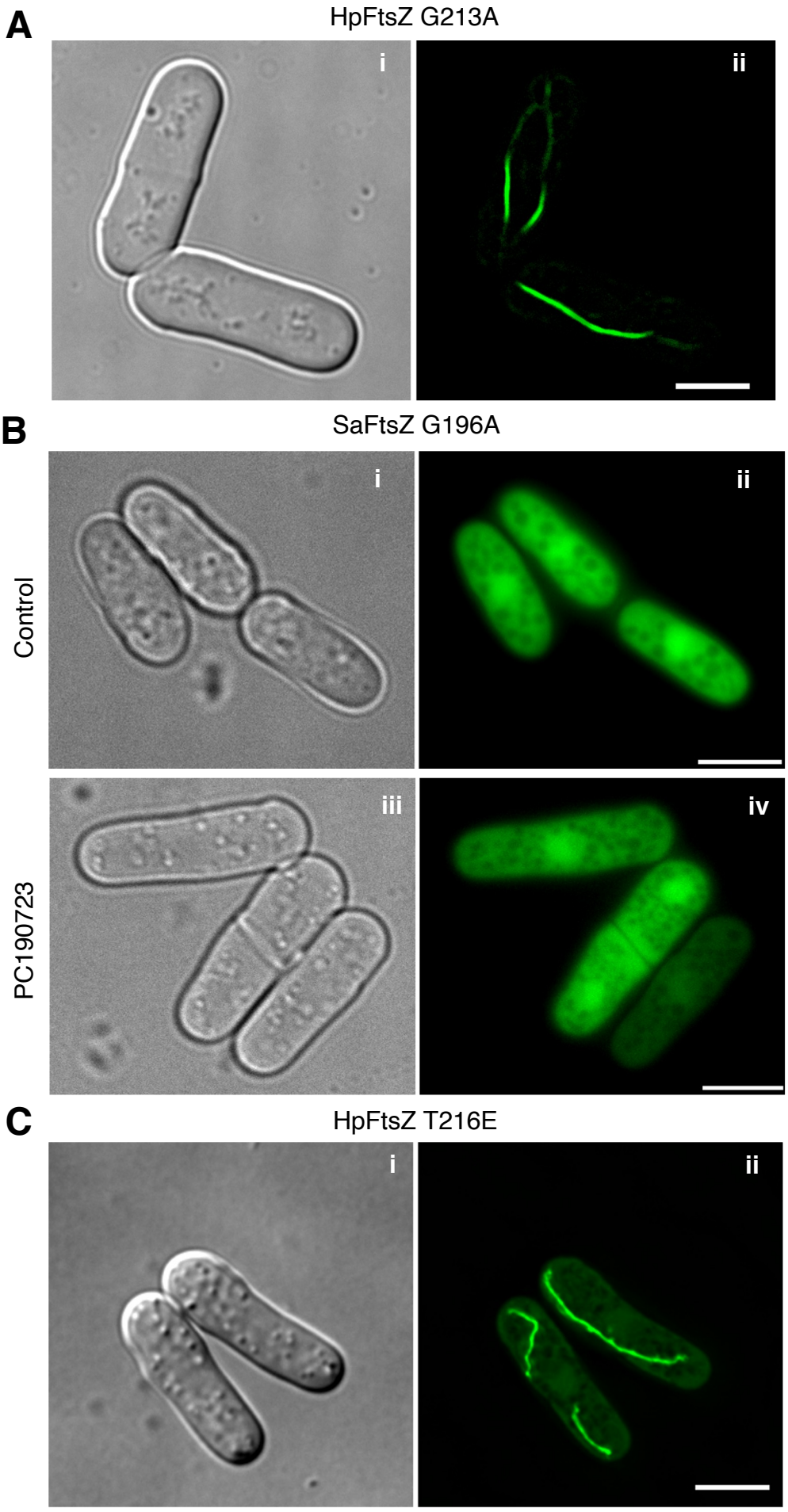
A
HpFtsZ G213A
i
ii
B
SaFtsZ G196A
Control
i
ii
PC190723
iii
iv
C
HpFtsZ T216E
i
ii

Figure S5. Assembly of FtsZ mutants resistant to PC190723 in fission yeast. **(A)** HpFtsZ mutation G213A that makes it resistant to the drug PC190723 is capable of polymerisation and assembly into filaments in fission yeast. **(B)** SaFtsZ^{G196A} fails to assemble into spots or patches either in the absence of the drug (panel ii) or in the presence of 20 μg / ml PC190723 (panel iv). **(C)** HpFtsZ mutant T216E, which is resistant to the drug PC190723 is capable of polymerisation and assembly into filaments in fission yeast. *S. pombe* cultures carrying pREP42-HpFtsZ^{G213A} or pREP42-HpFtsZ^{T216E} were grown for 10 – 12 hours and then sub-cultured into media containing PC190723 or equivalent volume of DMSO. They were further grown at 30°C for 4 hours to allow the expression of the proteins and imaged under the epifluorescence microscope. Scale bar represents 5 µm.

Supplementary Table – S1

List of strains and plasmids:

Strains/ Plasmids	Description	Reference
Yeast Strains		
CCDY3	MBY3497; CCDY346/pREP42- EcFtsZ-GFP	Srinivasan et al., 2008
CCDY4	MBY3532; CCDY346/pREP42- GFP-EcMreB	Srinivasan et al., 2007
CCDY340	CCDY346/pREP42- SaFtsZ-GFP	This work
CCDY341	CCDY346/pREP42- HpFtsZ-GFP	This work
CCDY346	MBY192; *Schizosaccharomyces pombe* [*ura4*-D18, *leu1*-32, h-]	Dr. Mithilesh Mishra (DBS, TIFR)
CCDY375	CCDY346/pREP42- HpFtsZ-G213A-GFP	This work
CCDY376	CCDY346/pREP42- SaFtsZ-G196A-GFP	This work
CCDY404	CCDY346/pREP42- HpFtsZ-T216E-GFP	This work
Bacterial Strains		
CCD190	DH10B; F – *mcrA* Δ(*mrr-hsdRMS-mcrBC*) φ80*lacZ*ΔM15 *ΔlacX74 recA1 endA1 araD139* Δ (*ara-leu*)7697 *galU galK* λ– *rpsL*(StrR) *nupG*	Invitrogen
CCD249	*Staphylococcus aureus* ATCC 25923	Lab Stock
--	*Helicobacter pylori* 26695	Dr. Asima Bhattacharyya
Plasmids		

pCCD4	pREP42- EcFtsZ-GFP	Srinivasan, et al. 2008
pCCD51	pREP42C- GFP	This work
pCCD712	pREP42- HpFtsZ-GFP	This work
pCCD713	pREP42- SaFtsZ-GFP	This work
pCCD716	pREP42- SaFtsZ-G213A-GFP	This work
pCCD753	pREP42- HpFtsZ-G196A-GFP	This work
pCCD838	pREP42- HpFtsZ-T216E-GFP	This work

Supplementary Table – S2

List of oligonucleotides:

RSO73	5' GCCTCCCCCGGGAACAACAACAACGCTAGCATGAGTAAAGGAGAAGAACTTTTC 3'	Forward primer for GFP (with SmaI site) used for creating pREP42C-GFP
RSO74	5' TTATTTGTATAGTTCATCCATGC 3'	Rev primer for GFP_STOP
RSO468	5' ATAGTCGCTTTGTTAAATCATATGGTTCATCAATCAGAG 3'	Forward primer having NdeI site for cloning of HpFtsZ
RSO469	5' AGCGTTGTTGTTGTTCCCGGGATCCTCATTGTCTTGCTGGATTC 3'	Reverse primer having BamHI site for cloning of HpFtsZ
RSO470	5' ATAGTCGCTTTGTTAAATCATATGTTAGAATTTGAACAAGGATTTAATC 3'	Forward primer having NdeI site for cloning of SaFtsZ
RSO471	5' AGCGTTGTTGTTGTTCCCGGGATCCTTATTACGTCTTGTTCTTCTTG 3'	Reverse primer having BamHI site for cloning of SaFtsZ
RSO650	5' GCTGTGAGTGCCATTTCTACTATCATCACTAAACC 3'	Forward primer for cloning of G213A_HpFtsZ
RSO651	5' GTAGAAATGGCACTCACAGCCCTAACCAAG 3'	Reverse primer for cloning of G213A_HpFtsZ

RSO648	5’ GTGTACAAGCTATCTCAGACTTAATCGCTGTTTC 3’	Forward primer for cloning of G196A_SaFtsZ
RSO649	5’ CTGAGATAGCTTGTACACCTTGGCGTAAC 3’	Reverse primer for cloning of G196A_SaFtsZ
RSO808	5’ GCATTTCTGAGATCATCACTAAACCCGG 3’	Forward primer for cloning of T216E_HpFtsZ
RSO809	5’ GTGATGATCTCAGAAATGCCACTCACAG 3’	Reverse primer for cloning of T216E_HpFtsZ

Supplementary Table – S3

List of reagents and chemicals

Reagents	Manufacturer/ Catalog No.
LB medium	(Difco – 244620)
Brucella broth	BD 211088
Fetal bovine serum	HiMedia – RM9970
Carbenicillin	Sigma – C1389 or MP Biomedicals - 0219509201
Kanamycin	Sigma – 60615
Chloramphenicol	Sigma – C0857
YES Agar	Formedium™ - PCM0410
YES Broth	Formedium™ - PCM0310
Edinburg minimal medium (EMM Agar or EMM Broth)	Formedium™ - PMD0210
Adenine	Formedium™ - DOC0229
Histidine	Formedium™ - DOC0144
Leucine	Formedium™ - DOC0157
Uracil	Formedium™ - DOC0214
Thiamine	Sigma - T4625
PC190723	Merck - 344580
Sanguinarine	Sigma - S5890
Berberine	Sigma - B3251
DMSO	Sigma - 317275
Genomic DNA Isolation kit	HiMedia Labs - MB505
Q5 Polymerase	NEB - M0492S

96-well plate	Corning - CLS3370